An explanatory model for the burial of fines in the sandy seabed of the southern North Sea

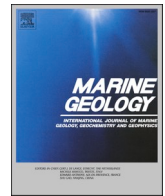Hendriks, E.; van Prooijen, B. C.; Cheng, C. H.; Aarninkhof, S. G.J.; Winterwerp, J. C.; Soetaert, K. E.

Important note
To cite this publication, please use the final published version (if applicable).
Please check the document version above.

Research Article

An explanatory model for the burial of fines in the sandy seabed of the southern North Sea

E. Hendriks [a,b,*], B.C. van Prooijen [a], C.H. Cheng [c], S.G.J. Aarninkhof [a], J.C. Winterwerp [a], K.E. Soetaert [d]

[a] Delft University of Technology, Faculty of Civil Engineering and Geosciences, Department of Hydraulic Engineering, Delft, the Netherlands
[b] Deltares, Unit of Marine and Coastal Systems, Department of Ecosystems and Sediment Dynamics, Delft, the Netherlands
[c] Wageningen Marine Research, Yerseke, the Netherlands
[d] Royal Netherlands Institute for Sea Research, Department of Estuarine & Delta Systems, Yerseke, the Netherlands

ARTICLE INFO

ABSTRACT

The amount of suspended fines in the southern North Sea strongly depends on their exchange with the sandy seabed. This exchange is governed by resuspension of fines during storms, followed by burial in the week thereafter. Despite its importance for fine sediment dynamics, the burial of fines into a sandy seabed is currently not well understood. This paper presents a mechanistic conceptual model, explaining how the interaction of migrating small ripples and larger megaripples can bury fine sediment in a sandy seabed shortly after storms. The burial process consists of four phases forming a dynamic cycle. A storm stirs up the bed, remobilising fines, while forming megaripples. After the storm, fines can settle again depositing atop the sandy seabed. Interaction between bedforms of different scales is then crucial to bury fines 1–2 dm within the seabed. Megaripples formed during storms gradually adjust to calmer conditions in the waning of storms. During this adjustment period, fines are buried by current-induced ripples in the troughs of the former megaripples. Field measurements collected in 2017 corroborate this conceptual model, showing fines in distinct patches, both horizontally and vertically. Furthermore, fines are found up to 10–15 cm in the seabed shortly after storms. The data further reveal how fine sediment occurrences on and within the seabed vary strongly over multiple length scales. They both vary on the mega-scale (kilometres) and on the micro-scale (metres-centimetres). As the micro-scale is multiple orders of magnitude smaller than the scale on which hydro-morphological models operate, parameterisations are required to aggregate the effect of burial in numerical models.

1. Introduction

Shallow seas are more and more exposed to human interferences (Degraer et al., 2019), like beam trawl fishing (Rijnsdorp et al., 2008), dredging for land reclamation (Stolk and Dijkshoorn, 2009) and construction of offshore wind farms (Breton and Moe, 2009). These interferences lead to a modification of the suspended sediment concentration (SSC) (Piet et al., 2019). Most suspended sediment consists of fine sediment (i.e., fines, sediment smaller than 63 μm), which plays a major role in the ecological functioning of shallow coastal seas. When suspended in the water column, fine sediment leads to an increase in turbidity (Fettweis et al., 2019), thereby hampering sunlight penetration into the water (Kirk, 1994). This may lead to a decrease in

phytoplankton growth rate (e.g., Anthony et al., 2004; Van Duin et al., 2001) and thus a decline in ecosystem health, as phytoplankton form the base of the marine food pyramid. In this paper, we focus on the southern North Sea, where ecosystem functioning is strongly influenced by fine sediment dynamics (van der Molen et al., 2017), even though its seabed is predominantly sandy.

In the southern North Sea, SSC varies strongly in both time and space. On short temporal scales, it depends on the occurrence of storms (Stanev et al., 2009; van der Hout et al., 2017). During storms, a simultaneous increase in SSC occurs in the entire southern North Sea within days of the storm onset (Fettweis et al., 2012; Pietrzak et al., 2011; Suijlen and Duin, 2001). Subsequently, SSC steadily decreases, while still varying on tidal timescales (Flores et al., 2017; van der Hout

et al., 2017). Within a week, SSC in the entire area has again decreased to pre-storm values (Fettweis et al., 2010; Suijlen and Duin, 2001; van der Hout et al., 2017). Spatially, mean SSC mainly depends on cross-shore distance (de Boer et al., 2009). Concentrations are generally high within 2–3 km from the shore, strongly decreasing in an offshore direction (Fettweis and van den Eynde, 2003; van Alphen, 1990; van der Hout et al., 2015).Both the temporal and spatial variations indicate that SSC magnitude strongly depends on the exchange of fines with the sandy seabed (van Kessel et al., 2011; van Prooijen et al., 2007). The simultaneous increase of SSC during storms over a large domain can only be explained from local sources of fines throughout the system. Advection, dispersing sediment from one or a few isolated sources, is too slow of a process to explain the quasi-instantaneous increase of SSC over this large domain. Likely, these local sources consist of fines which are remobilised from the seabed by waves (Fettweis et al., 2010; Flores et al., 2017). The system-wide decrease in SSC within a week after a storm suggests local sinks of fines within the system, forming the SSC source for the next storm. During calm conditions, fines settle out of suspension and deposit. Due to their small settling velocity, they deposit on top of the sandy seabed. As tidal currents resuspend fines into the water column when they are readily available on the seabed (Terwindt and Breusers, 1972; van Maren et al., 2020; Widdows et al., 2007), a decrease in SSC implies that they are no longer available, but are buried within the seabed. Thus, burial in the seabed provides local sinks for fines. This short-term water-bed exchange leads to considerable short-term variations in fines percentage in the southern North Sea bed (Hendriks et al., 2020; Witbaard et al., 2013). However, it does not affect the fines percentage in the upper strata of the North Sea bed on decadal time scales (Eisma, 1968; Hendriks et al., 2020; van Alphen, 1987a).

Despite its importance for fine sediment dynamics, the burial of fines into a sandy seabed is currently not well understood. A mechanistic description is lacking for this process, thus only heuristic burial parameterisations are used in the literature (Sanford, 2008; van Kessel et al., 2011). This limits the modelling of fine sediment dynamics in shallow coastal seas (van Maren et al., 2020). To improve this, a conceptual description for the burial of fines is required.

Previous research suggests three possible processes which may bury fines into the seabed, but for none of these a mechanistic description is available. These processes are: (1) pore water flow induced by pressure gradients over bedforms, (2) bioturbation and (3) bedform migration (Dankers, 2005; Eisma, 1968; Graf and Rosenberg, 1997; Huettel et al., 1996; Huettel and Rusch, 2000; Jennes and Duineveld, 1985; Le Hir et al., 2007; Martinius and van den Berg, 2011). Pore water flow rates are generally small, and only make a considerable contribution in coarse sediment where pressure gradients are large (Harrison et al., 1983; van der Loeff, 1981; Webb and Theodor, 1968). Hence, it is expected that they hardly bury fines in the southern North Sea bed, with median grain sizes (d_{50}) of 200–350 μm, even over long timescales (Kleinhans et al., 2005). Bioturbation is an effective mixing mechanism (Graf and Rosenberg, 1997; Kleinhans et al., 2005; Kristensen et al., 2012; Le Hir et al., 2007; Volkenborn et al., 2007; Witbaard et al., 2016), but is only able to accumulate fines over longer timescales, on the order of weeks to months, or even years (Kleinhans et al., 2005; Lecroart et al., 2007; Middelburg et al., 1997). As there are no indications of increased biogenic activity after storms, bioturbation will not lead to sufficient burial of fines in the days after a storm. This leaves bedform migration as the only likely mechanism for the considered area.

The objective of our work is to develop a conceptual mechanistic model explaining the burial of fines into a sandy seabed induced by the formation and migration of bedforms. This model is inspired by in-situ observations in the North Sea, and its development was an iterative process in concert with analysing the data. To properly assess the data, one needs to be informed by the conceptual model. Therefore, we start by introducing this model in Section 2, which provides a phenomenological description of the burial process. It has been deduced from an analysis of the relevant bedforms in the North Sea, and sedimentological

theory on flaser bedding (Reineck and Singh, 1980). Subsequently, the data collected in the North Sea are presented (Section 3). Using these data, we verify and discuss the proposed burial model (Section 4). Finally, we discuss the implications of our findings and present our conclusions (Sections 5 and 6). This paper only discusses the ingress of fines into a sandy seabed, not the remobilisation of fines from that seabed during a storm.

2. Bedforms and their role in fine sediment burial

2.1. Bedforms in the southern North Sea

A wide variety of bedforms is found on the southern North Sea bed (Passchier and Kleinhans, 2005), formed by the interaction between hydrodynamic forcing and the seabed (Damen et al., 2018; Hulscher and van den Brink, 2001). Both the hydrodynamic forcing and seabed characteristics vary in space and time and, as do the resulting bedforms. Their length varies from multiple kilometres (i.e., mega-scale) to
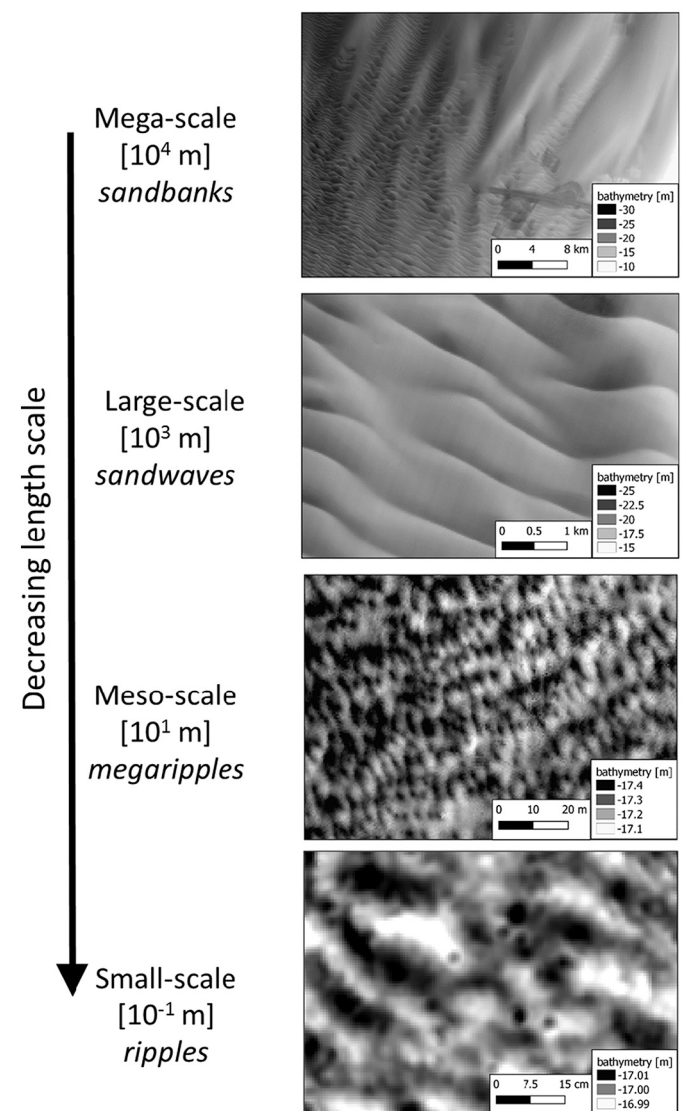
Fig. 1. Bedforms on different length scales along the Dutch coast. Length scales vary from 10^4 m (top panel) to 10^{-1} m (bottom panel). Upper two panels from NLHO data (NLHO and Deltares, 2019). Lower two panels using data from the *Coastal Genesis 2.0* dataset (van der Werf et al., 2022). Top left corner of each map in ETRS89 UTM31N coordinates – I: (563,971, 5,837,427), II: (580,136, 5,805,159), III: (656,068, 5,927,954), IV: (584,832, 5,793,243).

decimetres (i.e., small-scale) (Fig. 1). Smaller bedforms may develop atop larger ones, hence the seabed topography may ultimately become quite complex (Kleinhans et al., 2005).

Bedforms can be formed by tidal currents and waves, or a combination of both. This affects their length, shape, and associated time scale. Mega- and large-scale bedforms (wave lengths larger than tens of metres) are predominantly current-induced and tend to be asymmetric (van Gerwen et al., 2018), while small-scale bedforms (wave lengths smaller than several metres) can be formed by either tidal currents, waves or a combination thereof (Brakenhoff et al., 2020). Once formed, bedforms are not static but tend to migrate, and then change both in form and size. Migration rates are inversely related to bedform size (Baas et al., 2000). While mega-scale bedforms only migrate on decadal timescales, small-scale bedforms can migrate multiple times their own length within hours to days (Lichtman et al., 2018).

From this wide range of bedforms, we propose that only small- and meso-scale bedforms are relevant for the burial of fines. As burial predominantly takes place within the week after a storm, the relevant bedforms should be mobile enough to migrate or change shape over the course of a few days. Seaward from the surf zone, bedforms longer than several decametres can partially transform (Houthuys et al., 1994), but do not migrate nor transform entirely on these short timescales. Hence, we will not consider these in our analysis. We thus only consider the small- and meso-scale bedforms, known as ripples and megaripples (Fig. 1 – lower 2 panels).

At this length scale, bedform size and shape vary strongly with time, due to wave and tidal flow (e.g. Amos et al., 1996; Li and Amos, 1999). Resulting (mega-) ripples and their characteristics are summarised in Table 1. On the lower shoreface of the southern North Sea, ripple height is a few centimetres during calm, i.e. tide-dominated, periods (Meirelles et al., 2016; Schrijvershof et al., 2019; van der Werf et al., 2022; Wengrove et al., 2017). When the wave- and current intensity increase, so do ripple length and height. Above a certain threshold, ripples transform to megaripples (Soulsby et al., 2012). For current-induced bedforms, this transformation occurs around a Shields value of 0.1 (Marten, 2010), while for wave-induced bedforms, this transformation occurs gradually as their length and height depend on the orbital excursion (Table 1). The height of storm-induced megaripples and ripples on the lower shoreface varies from 0.05 cm to 0.2 m (Wengrove et al., 2019, 2018). However, bedforms need time to adjust to the governing hydrodynamic conditions. Hence, the transformation from current-induced to storm-induced

bedforms is gradual (Soulsby et al., 2012; Traykovski, 2007). Likewise, the transition back to current-induced ripples is also gradual, and generally takes place within hours to several days (Wengrove et al., 2018).

2.2. Fines burial by a migrating ripple

We argue that small, current-induced ripples are the principal bedform type burying fines into a sandy seabed. This burial process is sketched in Fig. 2, showing a ripple cross-section. It presumes that ripples migrate in a single direction, with intermittent periods of slack water, and are two-dimensional. These presumptions aim to make the process description more straightforward. The first presumption is based on the fact that tidal currents along the Dutch shore are flood-dominated (Grasmeijer et al., 2022). As current-induced ripple migration rates scale non-linearly with flow velocity (Table 1), this asymmetry leads to a dominant migration direction. This is consistent with the findings of van der Werf et al. (2022), who showed that the critical Shields parameter is only occasionally exceeded on the Dutch lower shoreface by ebb currents alone. In reality, ripples will likely be three-dimensional and can also migrate in opposing directions. Though this may affect burial rates (quantitative) it will not affect the relevant processes (qualitative). Below, we elaborate on the different steps in the burial process.

Due to tidal currents, asymmetric current ripples of 2–3 cm high are formed in fine sand with a steepness of 0.06–0.1 (Fig. 2a) (Soulsby et al., 2012; van der Werf et al., 2022). Due to its asymmetry, flow separation occurs from the ripple crest (flow separation area indicated by the dash-dotted lines in Fig. 2). Hence, a wake forms at the steep lee side of the ripple. In this wake, the bed shear stress is (at least) 20% lower than on the crest (Fernandez et al., 2006; McLean et al., 1994). These ripples will migrate along the bed if the tidal currents are strong enough to exceed the critical Shields parameter.

During slack water, current velocities decrease and ripple migration ceases. Consequently, fines settle out of suspension and deposit on the seabed (Fig. 2b). The amount of deposited fines depends on the slack water duration, concentration of suspended fine sediment and characteristic settling velocity (Winterwerp, 2007). The largest net deposition is expected to occur on the lee side and in the ripple trough (Reineck and Wunderlich, 1968). As the in-situ density of suspended fines is relatively low (i.e. water content is high), a relatively thick, but soft layer of fines is expected to build up in the trough (Terwindt and Breusers, 1972). The critical shear stress for resuspending these freshly deposited fines is generally low, on the order of 0.1 Pa (van Kessel et al., 2011; van Maren et al., 2020; Widdows et al., 2007). This is lower than the critical shear stress for fine sand, which is approximately 0.2 Pa (van Rijn, 2007).

When the tidal current increases again, so does the bed shear stress. Fines on the lee side of the ripple are (partially) eroded because of their low critical shear stress. However, in the wake of the bedform and the induced return flow, part of the fines remains within the trough, also at larger flow velocities. When the bed shear stress exceeds the critical shear stress for sand, sand grains on the stoss side will be transported as bedload (Fig. 2c). As the bed shear stress is not uniformly distributed over the ripple, sand transport on the stoss side starts shortly after fines start to be eroded on the lee side. Once the sand grains are transported over the ripple crest, they deposit atop the fines still present in the trough. As more sand grains are transported, the ripple migrates.

After a short period of time, the ripple has migrated by distance x_{mig} and has buried some fines (Fig. 2d). Due to the load imposed by the overlying sand, the layer of fines consolidates. As a result, its density increases while the layer thickness decreases. These fines are buried in the upper seabed strata as individual lenses, and likely not mixed with the sandy substrate. This yields a flaser bedding, as described in sedimentology (Martin, 2000; Reineck and Singh, 1980; Reineck and Wunderlich, 1968; Terwindt and Breusers, 1972).

This process is relatively fast, as current-induced ripples can migrate several times their own length within a tidal cycle (Lichtman et al.,

Table 1

Ripple and megaripple characteristics based on dominant hydrodynamic forcing. Ripple properties: η_{eq} – equilibrium ripple height, λ_{eq} – equilibrium ripple length, v_{mig} – migration rate. Parameters: D_* – dimensionless grain size (e.g., van Rijn, 2007), d_{50} – median grain size, d_0 – near-bed orbital excursion, θ – Shields parameter, u_c – current-induced velocity and u_w – wave-induced velocity. The typical values are for fine sand, and for wave-induced bedforms only apply to orbital (mega-) ripples.

| Type -> Property	Current-induced ripples	Wave-induced	Combined wave-current
$\eta_{Eq.}$ [m]	$\eta_{eq} = d_{50} 202 D_*^{-0.554}$ (Soulsby et al., 2012)	$\eta_{eq} = 0.1 d_0$ (Wiberg and Harris, 1994)	$\eta_{eq} = \alpha 0.1 d_0$ where $\alpha = f(D_*, u_c, u_w)$ (Tanaka and Van Dang, 1996)
$\lambda_{Eq.}$ [m]	$\lambda_{eq} = d_{50} (500 + 1881 D_*^{-1.5})$ (Soulsby et al., 2012)	$\lambda_{eq} = 0.62 d_0$ (Wiberg and Harris, 1994)	$\lambda_{eq} = \alpha 0.62 d_0$ where $\alpha = f(D_*, u_c, u_w)$ (Tanaka and Van Dang, 1996)
Steepness (η_{eq}/λ_{eq}) [−]	0.06–0.1	Approx. 0.16	0.1–0.15
Shape [−]	Asymmetric	Symmetric	Asymmetric
v_{mig} [m/s]	$v_{mig} = 0.1154 \theta_r^{3.03}$ for $d_{50} = 238$ μm (Baas et al., 2000)	Depends on wave skewness (Traykovski et al., 1999)	Depends on wave skewness and θ (Amos et al., 1999)
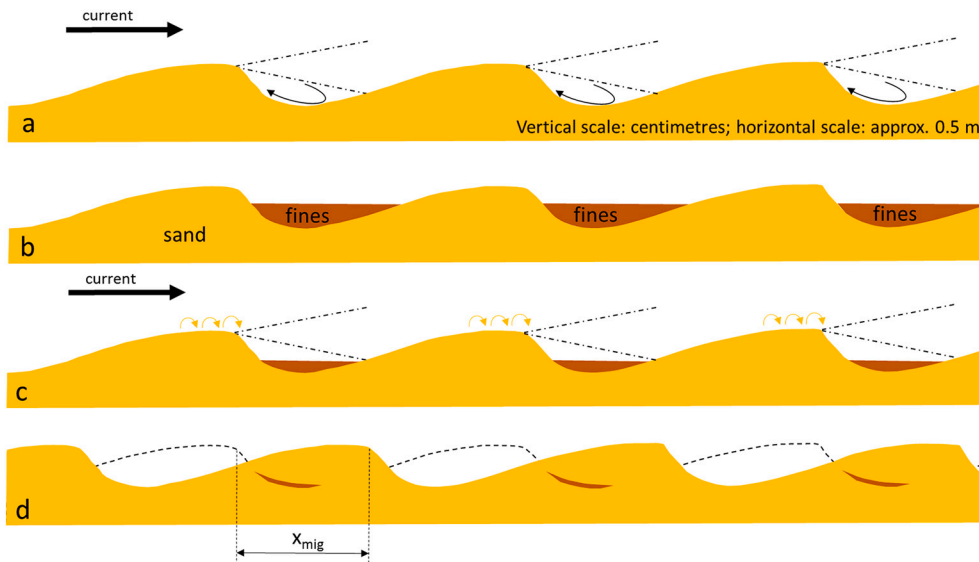
Fig. 2. Sketch of different steps for burial of fines by migrating small-scale bedforms. (a) Current-induced ripples migrating from left to right due to tidal current. Flow separation, indicated by the dash dotted lines, leads to a wake on the lee side of ripples. (b) During slack water, fines settle out of suspension, forming soft layers on the seabed. Largest net deposition is expected in the ripple troughs. (c) When tidal currents increase again, part of the previously deposited fines are eroded. Sand grains transported over the ripple crest deposit on the fines accumulated in the ripple troughs. (d) The ripples have migrated by distance x_{mig}, burying fines into the seabed. Fines are present as thin lenses.

2018). Because of the non-uniformity of bed shear stress over the ripple, this process explains why not all fines are eroded before they are covered by sand. However, the explanation provided here is not yet complete, for two main reasons. Firstly, due to the limited height of these ripples, fines would only be buried in the top centimetre of the seabed. Measurements indicate that fines are present not only in the top 1 cm, but are also found 10–15 cm below the seabed surface (Hendriks et al., 2020; Passchier and Kleinhans, 2005). Secondly, when the ripples migrate further than indicated in Fig. 2d, the fines which were previously buried at their lee side become exposed again at the stoss side within a short time. If the increase in critical shear stress of buried fines is limited, this would imply that only a little net burial would take place. Hence, an additional process must occur. In the next section, we hypothesise how the interaction between bedforms of different length scales leads to a net burial of fines.

2.3. Hypothesis: Burial due to interaction of scales

Interaction between bedforms of different length scales enables deeper burial of fines which therefore remain within the seabed for longer periods (i.e., between storms). As Fig. 1 shows, a multitude of different bedforms can occur on the North Sea bed, which can co-exist in
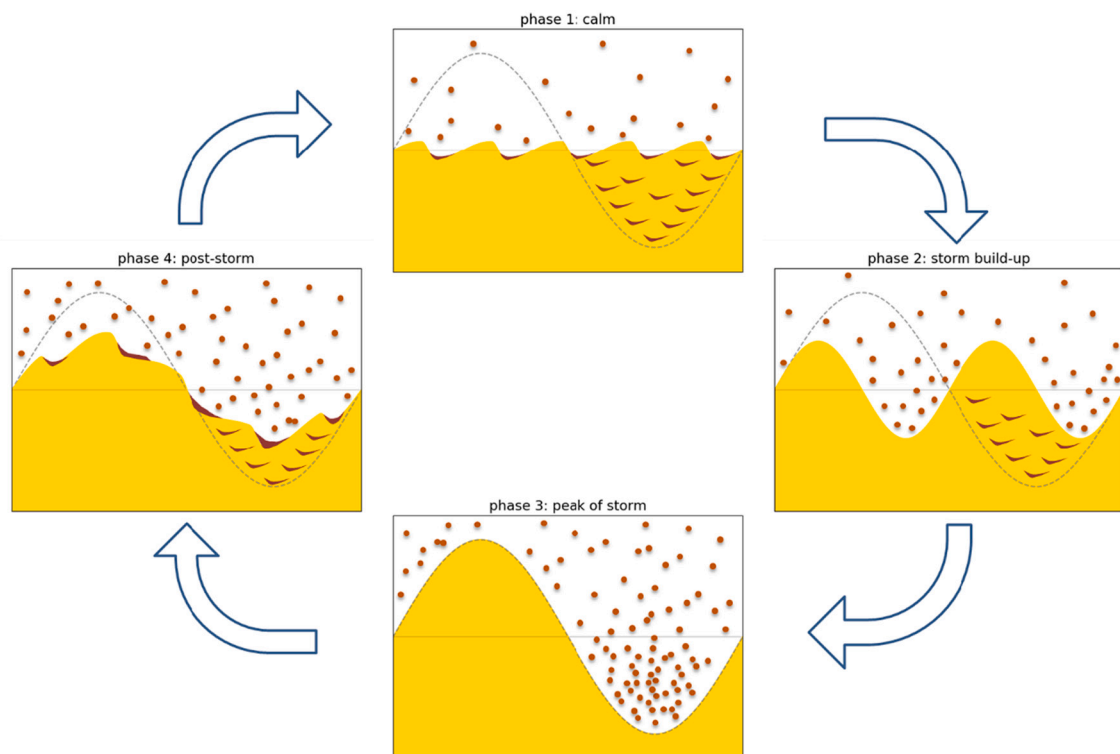
Fig. 3. Schematic of burial of fines in a sandy seabed due to reconfiguration and migration of larger and smaller bedforms. Yellow polygon indicates the sandy seabed. Brown lenses indicate fines in and on the seabed, while brown dots indicate suspended fines. Dashed grey line indicates maximum ripple dimensions formed during Phase 3. (For interpretation of the references to colour in this figure legend, the reader is referred to the web version of this article.)

both space and time. Bedforms of different scales, from mega- to small-scale, interact with one another. Our hypothesis elaborates on the interaction between bedforms of small- and meso-scale, i.e. ripples and megaripples (two lower panels Fig. 1).

This interaction is sketched in Fig. 3, which proposes four distinct phases in the burial process. Together, these form a dynamic cycle. For each phase, we discern between the behaviour of the sandy seabed and the presence of fines. The latter can either be suspended in the water column, deposited on, or buried within the seabed.

We start with Phase 1, which occurs in a relatively calm period, dominated by tidal currents. Only small current-induced ripples are formed on the seabed. Hence, the height of the active ripple layer is limited to 2–3 cm Most fines were buried in the seabed during previous cycles, deeper than this active layer. SSC is low and at slack tide, thin layers of fines deposit on the seabed, preferentially in the ripple troughs. The small-scale ripples migrate (similar to Fig. 2), but the exchange of fines is limited.

Phase 2 represents a storm build-up phase. Wave energy increases and wave-induced bedforms are formed on the seabed. These gradually develop into megaripples. During this phase, bedform height increases and fines are remobilised from the seabed. Since bed shear stresses are high, fines are not likely to deposit on the seabed. Thus, burial will be absent or limited. Combined, this leads to a net flux of fines into the water column and therefore an increase in SSC.

Phase 3 represents the storm peak, with maximal wave energy. The developed megaripples have reached their maximum height. We assume that these bedforms do not migrate substantially, owing to the symmetry of the waves. Most fines buried during the previous cycles have now been remobilised, leading to high SSC in the water column. As bed shear stresses are high, deposition of fines on the seabed is unlikely.

Phase 4 represents the post-storm phase, when wave energy is low again and tidal currents are dominant. Current-induced ripples form, superimposed on the megaripples. These ripples will migrate, leading to a net sand transport towards the megaripple troughs for two reasons. First, bed shear stresses on the stoss and crest of the megaripples are higher than on the lee side and troughs. Second, the bed elevation gradients lead to net sand transports (van Rijn, 1984; Walstra et al., 2007). As a result, the storm-induced megaripples gradually flatten out and the smaller ripples become dominant again.

Fines are buried into the seabed during Phase 4, because of the migrating small-scale ripples. Similar to Fig. 2, fines deposit in the troughs of the small-scale ripples during slack tide. Since SSC is still high due to the preceding storm, deposition rates will be high and a relatively thick layer of fines is formed. Subsequently, the fines are buried when the ripples migrate. Because of the asymmetry in sand transport, the ripples migrating towards the trough of the former megaripple will be covered by subsequent migrating ripples. In this way, fines end up at different depths in the bed and become unavailable for resuspension by the tidal currents.

This process generates distinct signatures of where and how fines are found in the seabed. Burial depth is contingent on bedform height, thus the maximum depth at which fines are buried depends on the height of bedforms created during storms. When fines have been buried in the seabed, they are present as distinct lenses. Furthermore, fines predominantly end up in the former troughs of megaripples and not in their crests. This implies that fines percentages vary substantially on megaripple length scales, from zero at the former megaripple crest to a high fines content in the former trough in the form of (multiple) lenses.

3. Materials and methods

3.1. Study site and measurement period

The conceptual model was developed and tested with data collected in the southern North Sea. As the seabed and water column form a coupled system, simultaneous measurements of both elements are

required. Seabed samples were taken along a cross-shore transect offshore of Egmond aan Zee, the Netherlands (Fig. 4a) in 2017. This transect starts at 1 km offshore (52.6371°N, 4.6054°E) and extends to 10 km offshore 52.6389°N, 4.4722°E). It is located approximately 80 km north of the River Rhine outflow, thus in the far-field region of the Rhine Region of Freshwater Influence (ROFI). Therefore, the water column at Egmond aan Zee periodically experiences weak stratification (Rijnsburger et al., 2016). It lies 20 km north of the port of IJmuiden, where no significant volume of freshwater is discharged into the North Sea. However, approximately 1 MT of dredged fine sediment is disposed of directly north of the harbour entrance channel annually (Winterwerp, 2001). This disposal site lies 15 km south of the studied transect, and fines deposited there will eventually reach the Egmond aan Zee transect as the residual transport direction of fines along the Dutch coast is in north-easterly direction (de Boer et al., 2009).

The seabed along this transect is mostly sandy, with a d_{50} of 200–250 µm and a fines percentage of up to 10% (Witbaard et al., 2016). A net shoreward transport of fine sediment exists during calm periods (van der Hout et al., 2015), inducing elevated levels of turbidity between 1 and 3 km from the shore (van Alphen, 1990; van der Hout et al., 2015). Morphologically, the area is characterised by the presence of several shoreface-connected ridges (van de Meene and van Rijn, 2000). The bed level along the transect varies from −10 m to −20 m (Fig. 4b), situating it entirely on the lower shoreface (Anthony and Aagaard, 2020; Grasmeijer et al., 2022). All bed levels are referenced to the Dutch Ordnance level (NAP, *Nieuw Amsterdams Peil*).

The first sampling campaign took place from 9 to 11 June 2017 and the second from 19 to 26 October 2017. In the remainder of the text, we refer to them as the 'June' and 'October' campaigns, respectively. These campaigns were performed using the RV Pelagia of the Royal Netherlands Institute for Sea Research (NIOZ). During both campaigns, multiple measurements were done along this transect, comprising seabed sampling and measurements from instrumented landers. The applied techniques and data postprocessing are discussed in Sections 3.2 and 3.3.

3.2. Seabed sampling

The seabed was sampled at predefined stations along the transect (Fig. 4b) using two methods. The first method was the Multicorer (MC), which simultaneously collects up to 8 bed sediment samples at a station. The MC was deployed at 1000-m intervals in both campaigns. The second method, Sediment Profiling Imagery (SPI), was used to take images of the upper seabed layer. The SPI stations were evenly spaced at 500-m intervals in June and October (Fig. 4b). However, in the latter campaign, we adjusted the spacing of the stations in the most offshore 5 km part of the transect to a 1000 m interval, as preliminary results from the June campaign showed more fines within the inner 5 km. This allowed us to sample the stations within 5 km twice. As the vessel was not equipped with Dynamic Positioning, seabed samples from the same station were not collected exactly at the same position in June and October but 10 to 30 m apart.

A standard protocol was followed to collect sediment samples with the MC. The device is equipped with eight 10-cm diameter cores (see Fig. 5b for image of MC frame). These are arranged in a fixed layout of two rows (Fig. 5c), which are 45 cm apart. Within a row, the centres of adjacent cores are 15 cm apart.

At least six sediment cores were required per station. Three of these were used to determine the grain size distribution, while the other three were used to determine substrate permeability (Cheng et al., 2020). In this paper, we only discuss the grain size distribution results. Cores with >10 cm of sediment were processed. If not enough cores of sufficient length could be collected within a single MC deployment, sampling was repeated until at least six sediment cores of sufficient length were collected. Additional sampling locations were located within 20 m from the initial location and taken within 30 min after the first deployment.
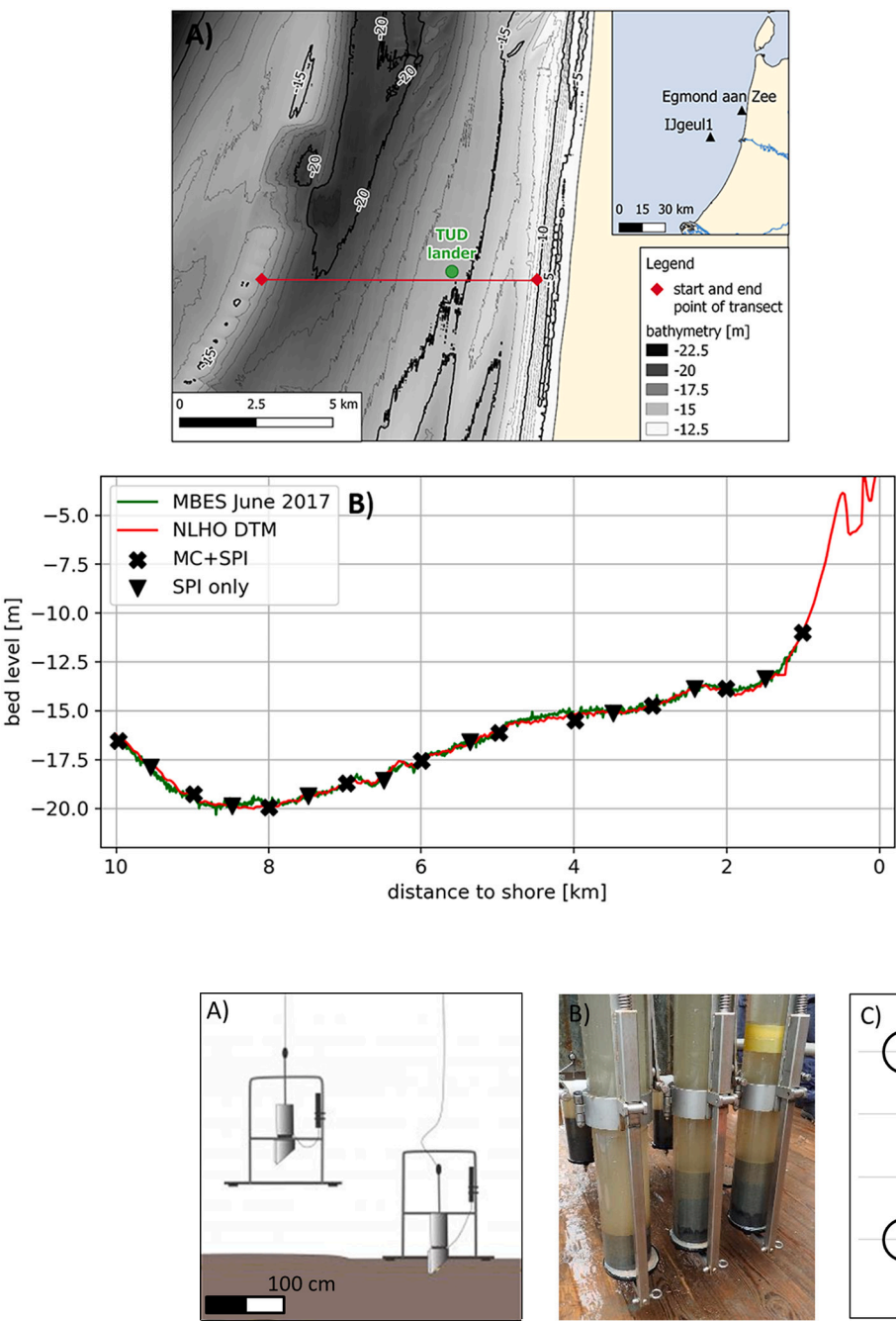
Fig. 4. (A) Egmond aan Zee cross-shore transect. Bathymetry based on NLHO Digital Terrain Model (DTM), based on bathymetric surveys from 2009, 2012 and 2014 (NLHO and Deltares, 2019). The inset indicates the location of the study site along the Holland coast and the location of the wave buoy IJgeul 1. (B) Bed level along the transect as determined from the NLHO DTM and multibeam echosounding during the campaigns, also indicating the seabed sampling stations for both Multicorer (MC) and Sediment Profiling Imagery (SPI).
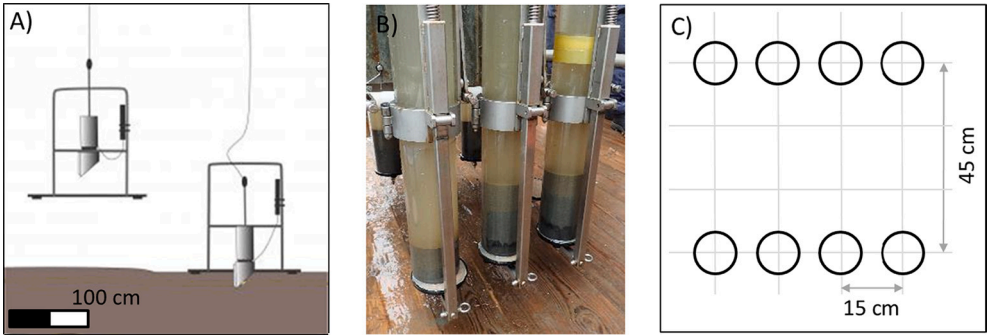

Fig. 5. (a) SPI deployment sketch (VLIZ 2022), (b) Photo of Multi Corer with collected sediment samples, (c) MC array with indication of dimensions.

The total number of MC deployments per station is listed in Table 2.

Once the sediment cores were retrieved from the MC, the overlying water was siphoned off carefully, without disturbing the sediment interface. The main cores were then subsampled using smaller acrylic tubes (length 15 cm, diameter 3.5 cm). These sub-cores were sliced at 1 cm intervals for the upper 5 cm and at 2-cm intervals for the lower part.

Table 2
Number of MC deployments per sampling station.

km offshore	10	9	8	7	6	5	4	3	2	1
Number of MC deployments – June	1	1	1	1	1	4	1	3	4	1
Number of MC deployments – October	1	1	2	2	1	6	3	3	1	1

Sediment slices were stored in a freezer at −20 °C in labelled vials. After the campaign, these vials were transported to the NIOZ laboratory ensuring the sediment remained frozen. There, the subsamples were first freeze-dried for 48 h, followed by sieving over a 1 mm mesh. During sieving, the material was thoroughly homogenised and wetted in tap water. A small subsample was analysed with a Malvern Mastersizer 2000 particle sizer. This instrument determines the grain size distribution by laser diffraction (McCave et al., 1986), yielding the volume percentage of different size classes. The size class of particles smaller than 63 μm is referred to as fines. We do not distinguish between the clay and silt fractions. Similar to Callesen et al. (2018) and Hendriks et al. (2020), we assume that volume percentages are representative for mass percentages.

The SPI system consists of a camera held within a frame, initially developed by Rhoads and Germano (1982) (Germano et al., 2011).

Fig. 5a shows how the SPI system is deployed. Ten seconds after each landing on the seabed, the first photo is taken. A duplicate photo is taken ten seconds later. After collecting two photos, the SPI frame is hoisted up several metres and lowered again at several decametres from the first sampling point. Here, another two photos are collected before it is brought back up to the ship deck.

The SPI photos provide a profile of up to the top 30 cm of the seabed. For sandier beds, the depth to which the camera prism penetrates the bed reduces to 5–10 cm and sometimes even less. If the penetration depth of the SPI camera is limited, the SPI image provides a pseudo-3D image of the seabed-water interface, showing parts of the seabed surface located away from the SPI prism (Fig. 6). Furthermore, the impact of the frame when landing on the seabed likely redistributes part of the fines on the seabed.

SPI images were post-processed following a standard procedure, illustrated in Fig. 6. The original images (Fig. 6-1) were cropped to 60% of their original height, and the RGB colours were converted to greyscale. The histogram of these greyscale images was then normalised based on the greyscale intensity limits of the substrate. A grid was laid over the images to measure lengths and heights. These normalised greyscale images (Fig. 6-2) were then converted back to a coloured image (Fig. 6-3) by applying the *'seismic'* false colour map in *matplotlib* (Hunter, 2007). Normalisation and colouring of images made it easier to discern between fines and sand. In the coloured images, patches of fines show up as red, textureless patches (Fig. 6-3). The sandy substrate, on the other hand, is mainly light to dark blue. Each coloured image was then assessed using the criteria in Table 3, similar to Karakassis et al. (2002) and Romero-Ramirez et al. (2013), which enabled a quantitative assessment of the SPI images.

3.3. Instrumented landers

3.3.1. Deployment and configuration

At the beginning of both campaigns, multiple instrumented landers were deployed on the seabed to measure a variety of physical parameters. In this paper, we focus on the data collected with the *TUD lander* at 4 km offshore (June: 52.6400°N, 4.5644°E; October 52.6401°N,

Table 3

SPI image assessment criteria.

Criterion	Classification	Attribute
Penetration depth	N/A	Depth in cm
Fines on substrate	Yes/no	Thickness of deposited layer
Fines in substrate	Yes/no	Patchy/well-mixed

4.5651°E). At this location, the bed level is −15 m NAP. A suite of instruments mounted on the lander measured flow velocity, turbidity and small-scale bathymetry (Table 4). Flow velocity and turbidity were measured at multiple heights in the water column.

In June, the landers were retrieved from the seabed at the end of the campaign. In October, the landers were retrieved one day before the end of the sampling campaign because of workability conditions.

3.3.2. Postprocessing lander data

The two Acoustic Doppler Velocimeters (ADVs) both measured at a 16 Hz frequency. The ADV installed closest to the bed (measurement volume at 0.15 mab) operated in bursts of 10 min, measuring for 9 min and 50 s with a 10 s interval before starting a new burst, while the ADV at 0.30 mab operated in continuous mode.

Table 4

Instruments mounted on the *TUD lander*. Instruments measured at different heights, indicated in metres above bed (mab). This table only lists the instruments of which the data was used in this paper.

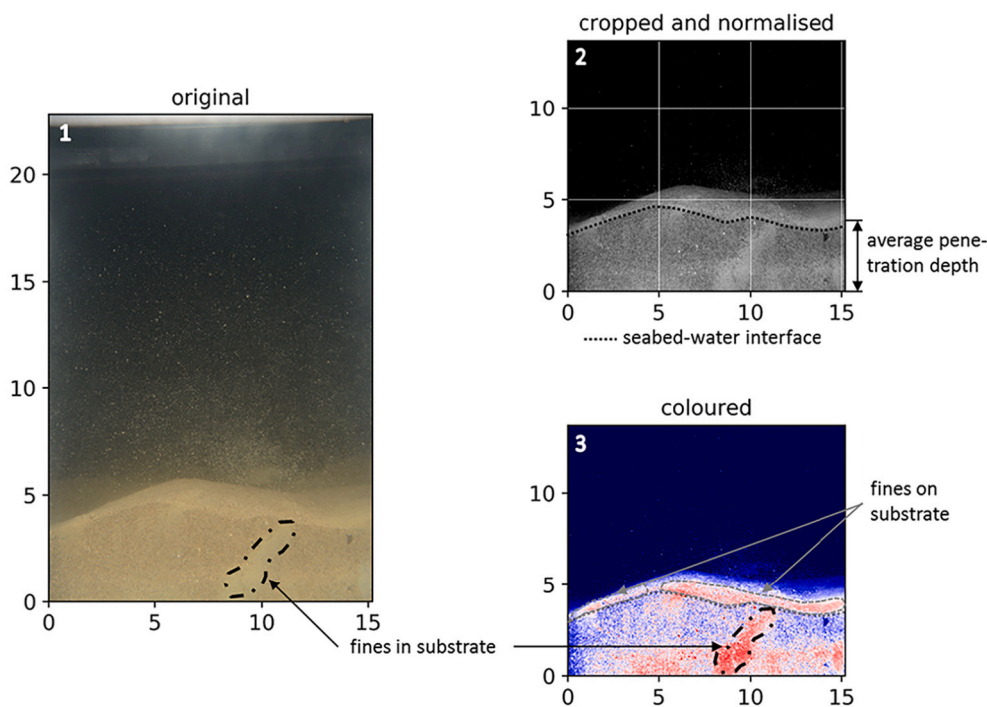| Instrument name	Measurement volume at (in metres above bed - mab)	Parameter	Period
Nortek Vector ADV	0.15, 0.3 mab	Velocity in single point	June & October
Campbell OBS 3	0.15, 0.3, 0.45, 0.6 mab	Turbidity	June & October
Marine Electronics Ripple Profiling Sonar	1.0 mab (sonar head)	Small-scale bathymetry	October

Fig. 6. SPI image processing. Original image (1) is cropped and normalised (2). Then coloured (3) using the *'seismic'* colour map, after which the fines in and on the substrate can be distinguished better. Assessment criteria are shown for each image. Original image taken in June 2017, at 2.5 km offshore.

Velocity timeseries were first corrected for pitch and roll of the lander, followed by a transformation from a local XYZ coordinate system to global ENU (East-North-Up) coordinates. The data were then filtered using a correlation and signal-to-noise (SNR) ratio mask (Elgar et al., 2005). Data points for which the beam correlation for all three ADV beams was below 80% and with an SNR smaller than 15 were removed from the data. If >30% of the samples within a moving 5-min window had to be filtered out, the entire 5-min window was removed. After filtering the data, the velocity time series were despiked (Goring and Nikora, 2002). Velocities were then rotated 6° in clockwise direction to obtain along-shore and cross-shore velocity components. Subsequently, the sign of the cross-shore velocity component was then reversed, so that it is defined as positive in the offshore direction.

The local bed elevation is determined from the ADV positioned at 0.15 mab, which recorded the distance to the seabed at the beginning of each 10-min burst. This data was filtered in two steps. First, values equal to zero were removed from the data. Second, a moving average with a time window of two hours was implemented. Values with an absolute difference larger than 4 cm from this mean were removed. Local bed elevation was then computed by subtracting the distance to the bed at the start of the deployment from the filtered signal.

Turbidity readings from the optical backscatter sensors (OBS) were calibrated for SSC using sediment-laden water samples collected at the Egmond aan Zee site. These samples were collected at the end of each campaign, stored in four 10-L buckets and transported to the TUDelft laboratory There, all OBS's were calibrated following the procedure by Colosimo et al. (2020). Concentrations were generally smaller than 1 g/l, hence a linear regression was sufficient to convert turbidity to SSC.

The ripple profiling sonar was used to obtain a small-scale 2D bathymetric map in the vicinity of the lander. The raw ping data from the sonar was converted to bed levels using the Bearing Direction Indicator method (Wengrove et al., 2017). These bed levels were then corrected for pitch and roll and interpolated to a regular grid with a 0.5 cm × 0.5 cm resolution. As the sonar head was positioned at 1.0 mab, and collected pings within a 150° arc, the maximum radius of the small-scale bathymetry was 3.8 m. Since the sonar steps through the swath at 0.9° increments, the resolution at the edges of the swath area is quite coarse. Hence, only the gridded data within a 2×2 m^2 area around the lander was used. A low-pass filter was then applied to remove the small-scale spikes deviating >10 cm from their direct surroundings. Missing values were interpolated using a linear interpolation from the nearest 5 cm in both directions. Finally, bedform heights and lengths were then computed using the 2D-spectral method of Wengrove et al. (2018).

4. Results

4.1. Hydro- and morphodynamic conditions

In June, the campaign took place several days after a fierce summer storm. During this storm, maximum significant wave heights of up to 4.5 m were measured at the nearby *IJGeul 1* wave buoy (Fig. 7c – grey hatch indicates campaign duration). During the storm, wave direction was west to southwest. Hydrodynamic conditions were calm during the campaign (Fig. 7b). Near-bed flow velocities (at 0.15 mab) show a semi-diurnal flood-dominant tide (Fig. 7a), with maximum along-shore velocities of 0.5 m/s and maximum cross-shore velocities of 0.15 m/s. Near-bed SSC shows a decreasing trend with peaks of up to 0.2 g/l on 09–06, and generally <0.1 g/l on the subsequent days (Fig. 7d). Note that the SSC signal at 0.15 mab overlaps with the 0.3 mab SSC signal in Fig. 7d. The SSC peaks seem uncorrelated with the tidal velocity, though some peaks occur during the peak ebb phase (dashed lines in Fig. 7a, d). Moreover, the local bed elevation (Fig. 7e) appears fairly constant throughout the measurement period, showing oscillations of 1–2 cm only during the peak flood phase.

In contrast, the campaign in October took place during a storm, with maximum wave heights of approximately 3 m at the *IJGeul 1* buoy
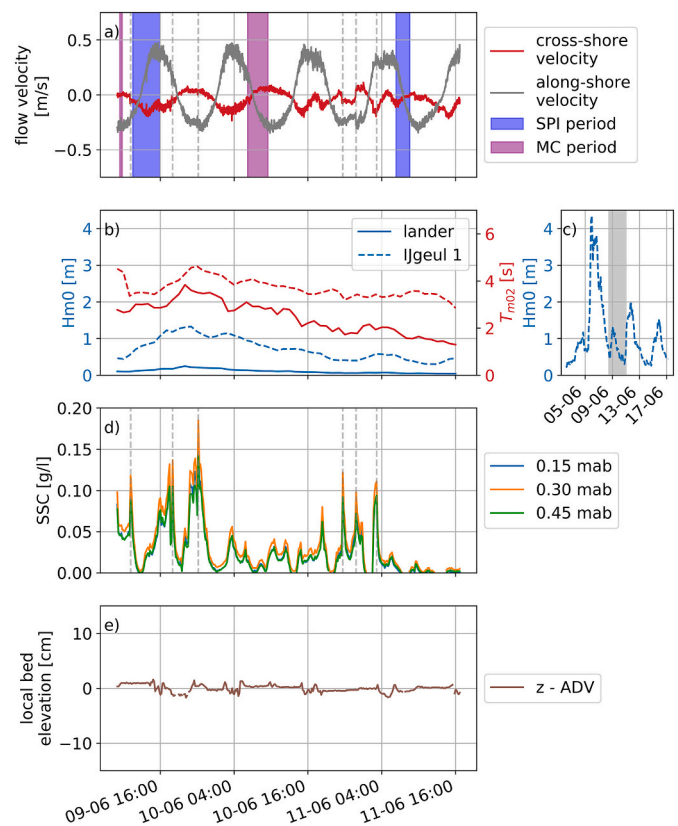

Fig. 7. Hydrodynamic conditions in June 2017. (a) ADV flow velocity; (b) wave heights and period during campaign at *TUD lander* and *IJgeul 1* wave buoy; (c) timing of campaign compared to wave height in June at *IJgeul 1* wave buoy; (d) SSC; (e) local bed elevation – ADV.

(Fig. 8c). Wave directions gradually varied over the course of the storm from southwest to northwest. While the velocity still has a semi-diurnal character, it is modulated by waves from 20 until 23 October (Fig. 8a, b). This leads to higher onshore velocities during the flood phase, together with a higher along-shore velocity. Ebb velocities decrease during the storm. Near-bed SSC increases from <0.05 g/l on 19–10 up to 0.7 g/l on 22–10 (Fig. 8d). Small-scale bathymetry suggests that the steep increase in SSC takes place shortly after the storm peak, roughly 2 days after the onset of the storm (Fig. 8e, f). The delay in SSC increase after storm onset is similar to the observations by van der Hout et al. (2017) at 1 km offshore from Egmond aan Zee. The subsequent SSC peaks mostly occur during the ebb phase, similar to the June measurement (dashed lines in Fig. 8a, d). These do not coincide with the peaks in local bed shear stress. A possible explanation could be the advection of fines from a nearby sediment patch. The preceding storm remobilised fines, which are not uniformly deposited in space. During the ebb phase, a larger amount of sediment could have been available for resuspension, even by weak tidal currents. There is no clear decrease in maximum SSC until the end of the measurement period.

The energetic conditions during the October campaign are confirmed by the local bed elevation as measured by the ADV (Fig. 8e – brown line). This varies strongly over the course of several hours to days. In the night from 21 to 10 to 22–10, local bed elevation increases from −3 to +9 cm. However, on 22–10 it decreases from +9 to −1 cm. These single point measurements cannot distinguish between vertical bed level changes in response to erosion/deposition or migration/reconfiguration of bed forms. The results of the ripple profiling sonar (see below) mainly suggest the latter.

Generally, the mean bed elevation measured by the sonar ($\bar{z}$) increased during the measurement period (Fig. 8e – blue line). It shows
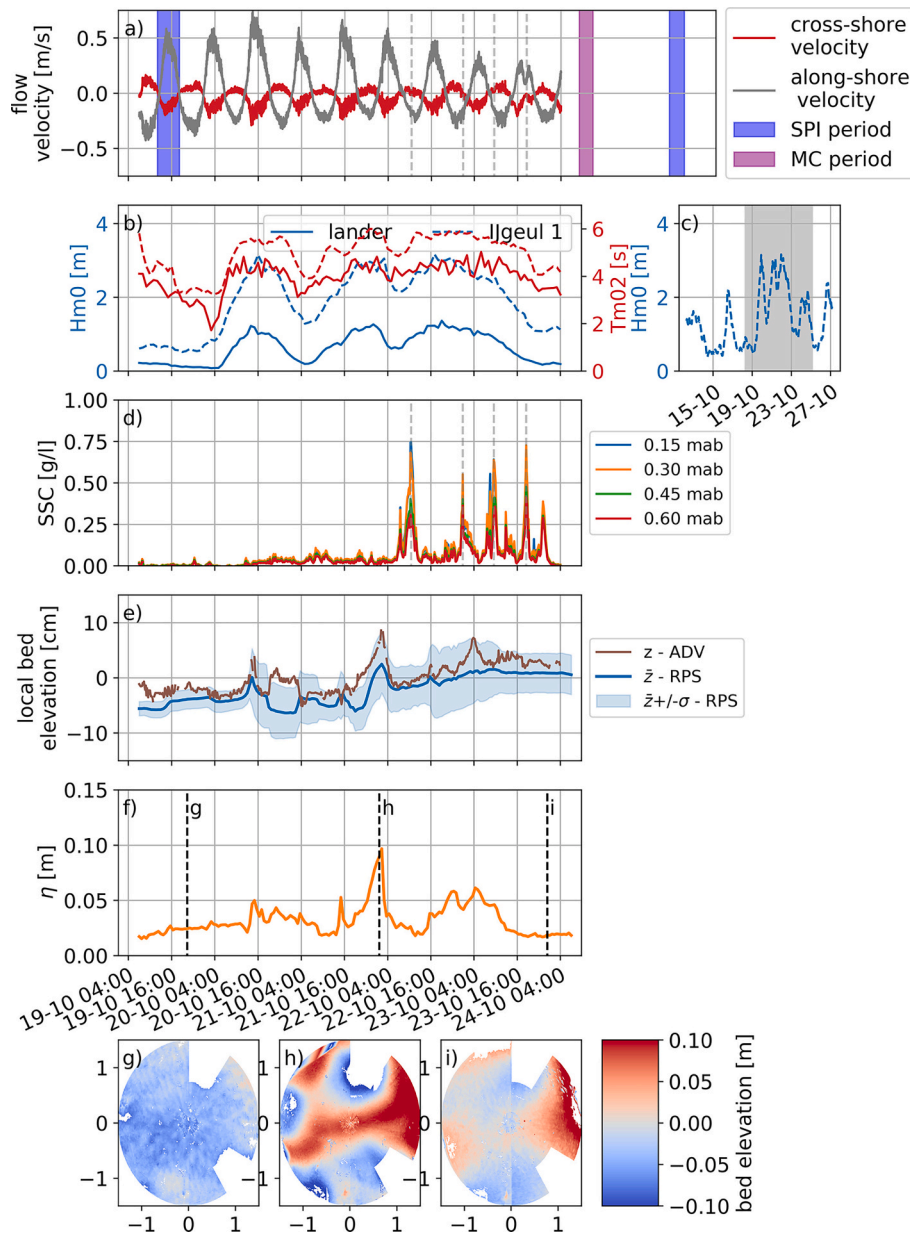
Fig. 8. Hydro- and morphodynamic conditions in October 2017. (a) ADV flow velocity; (b) wave heights and period during campaign at *TUD lander* and *IJgeul 1* wave buoy; (c) timing of campaign compared to wave height in October at *IJgeul 1* wave buoy; (d) SSC; (e) local bed elevation – ADV, mean bed elevation with standard deviations – ripple profiling sonar; (f) ripple height from elevation spectrum of sonar data; (g, h and i) small-scale bathymetry at three points in time.

similar trends as the bed elevation from the ADV, though the peaks are less pronounced. Before the onset of the storm, the ripple height (η) is generally small, i.e., 3 to 5 cm (Fig. 8f). During the storm, ripple height gradually increases to a maximum of approximately 0.1 m on 22–10 02:00. The maximum ripple height roughly coincides with the peak in local bed elevation (Fig. 8e). After reaching a maximum on 22–10, ripple heights first decrease strongly to 2 cm, then increase to 6 cm. In the wake of the storm, ripple heights are similar to pre-storm values, while the mean bed elevation under the sonar is still 5 cm higher (Fig. 8e).

In total, three sonar images collected before, during and after the storm (Fig. 8g, h, and i, respectively) to illustrate the seabed state. The blanked out areas in these sonar images represent removed data points; the colour map indicates the bed elevation. Before the storm, ripples are relatively short and are generally oriented from left to right (Fig. 8g). At the ripple height peak, the domain is almost entirely dominated by a few large storm-induced megaripples (Fig. 8h). These are longer and higher than the small-scale ripples. Their orientation is not clear since their

length scale is similar to the sonar footprint. Some scouring seems to have taken place directly left of the lander legs after the storm. After the storm, small-scale ripples can be observed again (Fig. 8i). These are oriented left-to-right and are superimposed on the decaying storm-induced bedforms. The contours of the latter are still visible in Fig. 8i, but much less pronounced than during the storm peak.

4.2. Trends in bed sediment composition

Fig. 7a and Fig. 8a depict when the seabed was sampled with the SPI and MC, in June and October, respectively. In October, MC samples and the second part of the SPI images were collected after the *TUD lander* had been retrieved. This means no direct sampling conditions are available, but the preceding conditions nevertheless provide a reliable estimate of these conditions (Fig. 8a).

First, we search for large-scale sediment distribution trends along the transect, comparing the results of both campaigns. In Fig. 9a, we show
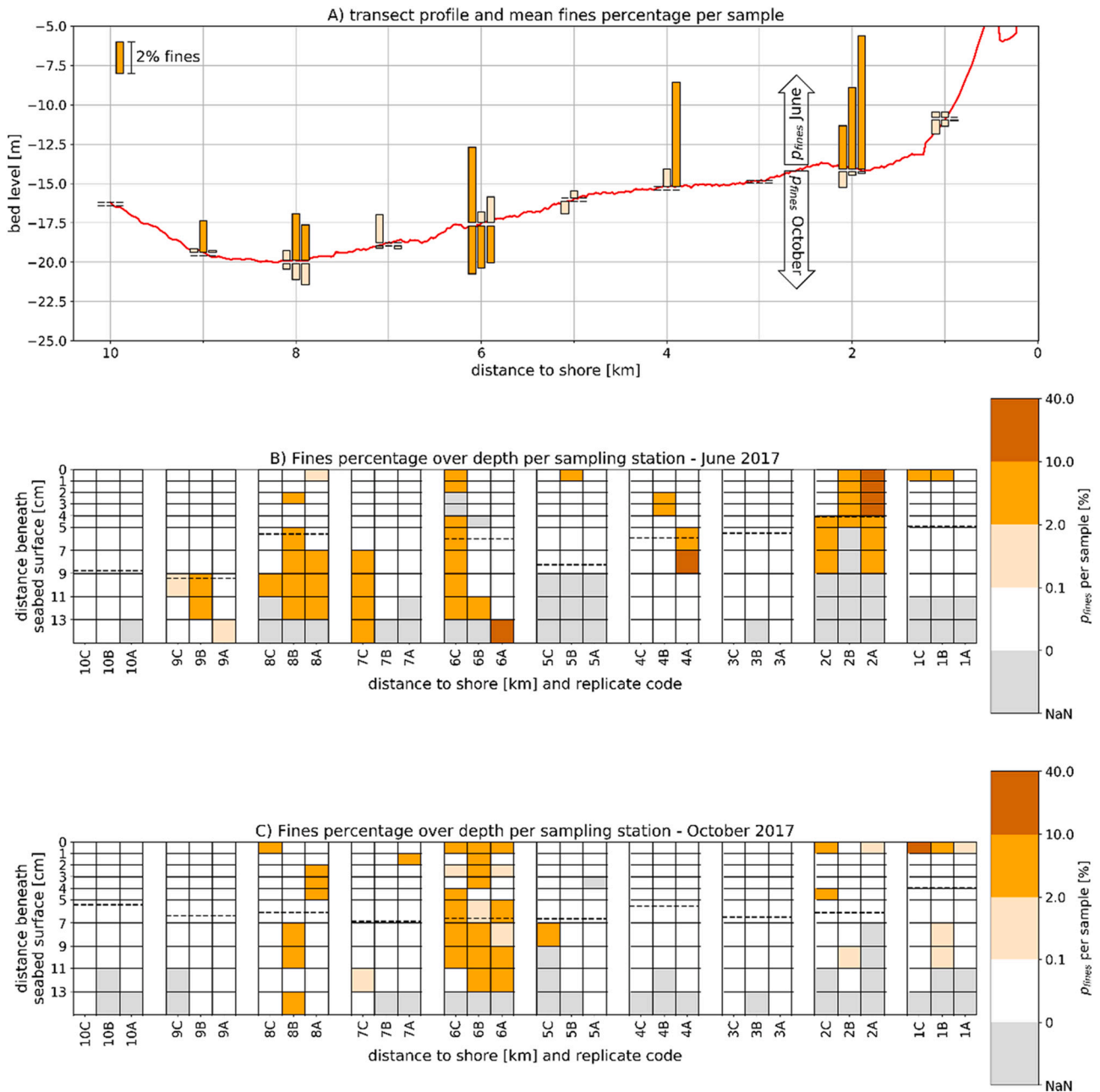
Fig. 9. (a) Mean fines percentage per sediment sample for both June and October, plotted along transect bed level (from NLHO digital terrain model). Mean percentage indicated by height of bar, 1 m = 1%. (b, c) Fines percentage in sediment slices collected in June and October, respectively. Slice colour indicates fines percentage, as per the classification of van Alphen, 1987a and Hendriks et al. (2020). Average penetration depth of the SPI per station is indicated with the dashed line.

the mean fines percentage (p_{fines}) for the three sister samples taken at the ten sampling stations along the transect. These samples are grouped per station and plotted at the corresponding distance to shore. The mean fines percentage of each sample is indicated by the height of the coloured bars. Those collected in June are plotted above the line representing the bed level (indicated with the red line) while those of October are plotted below this line.

In June, more samples contained fines than in October, 60% versus 50%, and p_{fines} was also higher. The conditional mean percentage, i.e. averaging only over the samples which contained fines, decreased from 2.4% in June to 1.0% in October. However, these averages are not representative for the fines distribution along the transect.

In addition, as Fig. 9a shows, fines percentages vary considerably on multiple spatial scales and over time. In June, the majority of the

samples had a mean fines percentage of 0–3%. However, maximum fines percentages per sample of up to 8.5% (2 km offshore), 6.7% (4 km offshore) and 4.8% (6 km offshore) were observed (Fig. 9a). In October, the mean fines percentage mostly ranged from 0 to 1.5%. The only exception are the mean fines percentages at 6 km offshore (bed level at −18 m), which ranged from 2.4 to 3.1%.

Moreover, the variation in mean fines percentage is not only observed between different stations, but also between sister samples collected at a given station (Fig. 9a). For instance, the mean fines percentage between sister samples from June varied from 0 to 6.5% (4 km), from 0.7 to 4.8% (6 km) or from 0.1 to 2.0% (9 km). As these sister samples were collected through a single MC deployment (Table 2), this means that fines percentages vary substantially within 0.5 m.

Similarly in October, the mean fines percentages between sister

samples differed from 0.1 to 1.0% (2 km) and 0 to 0.8% (5 km) (Fig. 9a). Absolute differences are smaller than in June, but relative differences are on the same order of magnitude. As these sister samples were collected through one or multiple MC deployments, the fines percentage at these stations varied either on a spatial scale of metres or decametres.

Fig. 9b and c present the fines presence of the upper 15 cm of the three sister samples taken at the 10 stations of Fig. 9a. Here, fines presence is defined as the mean fines percentage per 1-cm or 2-cm slice. This has been categorised according to van Alphen's classification (van Alphen, 1987a). The sister samples have been coded using the distance to shore and a letter. For instance, the third sister sample at 7 km offshore is marked '7C' (Fig. 9b).

Furthermore, Fig. 9b and c show that vertical variations in fines percentages are at least as pronounced as the horizontal variability. Most of the sediment slices contain no fines ($p_{fines} = 0$), but if they do contain fines, they usually fall within the 2–10% range. Only a few of the slices fall either within the 0–2% or >10% classes. As an example, we analyse the sister samples 4B and 4C, collected in June (Fig. 9b). In sample 4B, fines are only found at 2–4 cm below the seabed surface and these slices contain 8–9% fines. None of the other slices from this sample contained any fines. In sample 4C, fines are only found at 5–9 cm below the seabed. Here, the slice from 7 to 9 cm even contained 38% fines, while the slice underneath contained no fines. This heterogeneity is observed in both the June and the October profiles. The only station where the fines percentage over depth was relatively constant, was at 6 km offshore in October.

Above, we focused on specific trends per sampling campaign and general differences between the June and the October campaign. Comparing the results of both campaigns per station is disputable, as the length scale of fine sediment presence is of the same order as the positioning accuracy of the research vessel.

4.3. Small-scale seabed structure

The sediment sample data show how the presence of fines varies over multiple length scales, both in the horizontal and vertical directions. The SPI images contain additional information on the small-scale seabed structure. The average penetration depth of the SPI per station, as indicated in Fig. 9b and c with the dashed lines, was generally smaller than 10 cm. Within the width of the image, i.e. 15 cm, the presence and layering of sand and fines varies considerably. Examples of small-scale seabed structure are shown in Fig. 10, which includes SPI images taken in June, at 9.5, 4.0 and 2.0 km offshore.

From 10 to 8 km offshore the substrate is mostly sandy, judging by its texture and uniform sediment colour (Fig. 10a). Small-scale bedforms are observed in most images, with heights ranging from 1 to 3 cm. Generally, only very limited fines are present. Closer to shore, the sediment texture becomes less uniform. Patches of several cm wide are visible in the bed, having a texture different than the rest of the bed,

indicated in red colour (Fig. 10b). These are to be interpreted as patches of fines (Section 3.2). The water column above the bed is much richer in suspended sediment and the seabed topography is more irregular. At 1.5 and 2 km offshore, the most fines are observed, suspended and both on and in the seabed (Fig. 10c and Fig. 11). Fig. 10c exhibits two bedforms of at least 5 cm length (majority outside the picture), with the trough between them filled up with fines. The thickness of this deposited layer varies strongly over the small scale, from 2 cm to only several mm within a length of 10 cm (Fig. 10c), following the seabed topography. The maximum observed thickness is 4 cm, at 1.5 km offshore (Fig. 11 – right panel).

Fig. 11 shows two SPI images collected in June at 1.5 and 2.5 km offshore, within 30 min from each other. Even on the micro-scale of these images, the presence of fines on and in the seabed varies greatly.

In the left panel of Fig. 11, two patches of fines are buried in the top 2 cm of the seabed by overlying sand. These patches are similar to the lenses drawn in Fig. 2d, but oriented in the opposite direction. Their shape follows the profile of the asymmetric, current-induced ripples. The depth at which they are buried is larger than the current-induced ripple height, likely immobilising them until the next storm.

In contrast, the right panel of Fig. 11 shows the fines deposited in the trough of a small-scale bedform – in fact the entire trough is filled in. This small-scale bedform has a maximum height of approximately 4–5 cm, which is larger than current-induced ripples as the latter have a height of approximately 2 cm. This is possibly a relic bedform from the summer storm which preceded the June sampling campaign.

Fig. 12 quantifies the number of images where fines were either found on or in the substrate. It is formatted as Fig. 9a. Each bar along the transect indicates a station where SPI images were taken. As the number of SPI images differed per station, all bars were normalised by the total number of images taken at that station. Hence, all bars have equal length. These bars are coloured partly brown and partly white. The brown colour indicates the fraction of images in which fines were observed, while the white colour indicates the fraction in which they were absent. The bars above the bed level indicate fines on the substrate (such as Fig. 10c), while the bars below it indicate fines in the substrate (such as Fig. 10b).

In October (Fig. 12b), fines were rarely observed on the substrate along the entire transect. The only exception is the station at 1.5 km offshore. Furthermore, very little or no fines were observed within the substrate from 2.5 to 7 km. Closer than 2.5 km offshore and further than 7 km offshore, fines were regularly observed within the substrate.

Qualitatively, the presence of fines as determined from the sediment samples and SPI images agrees well. In 80% of the SPI images where fines are observed, they occur as distinct patches, which is also illustrated by Fig. 11. This confirms the fines presence observed in the sediment samples (Fig. 9b and c).

The results from June differ substantially from the October campaign. In June, fines were frequently observed on the substrate up to
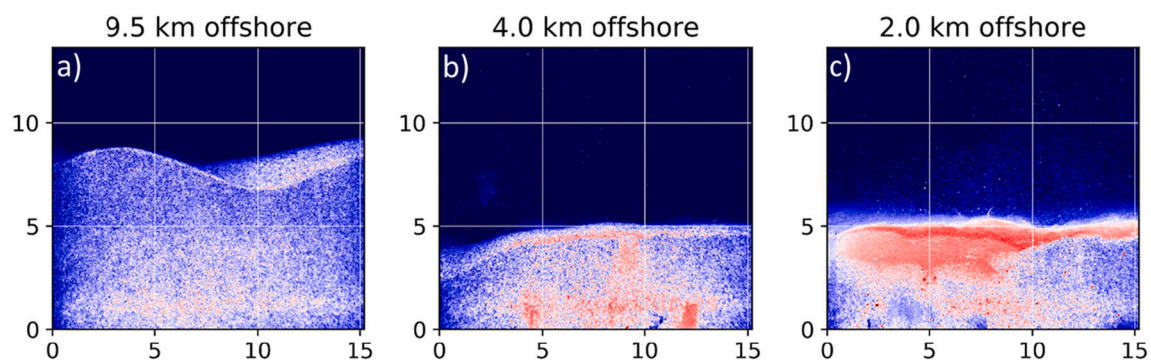

Fig. 10. SPI images taken during the June campaign at a) 9.5, b) 4.0 and c) 2.0 km offshore. The grid scale is centimetres. For an explanation of the colours, see Section 3.2.
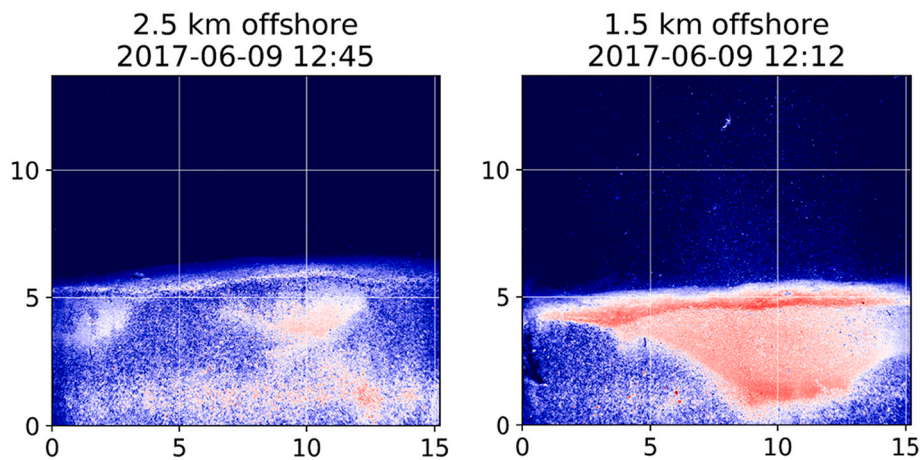
Fig. 11. SPI images taken at 2.5 and 1.5 km offshore, which show the interaction between fines and small-scale bedforms. This interaction leads to small-scale variations in the presence or absence of fines.
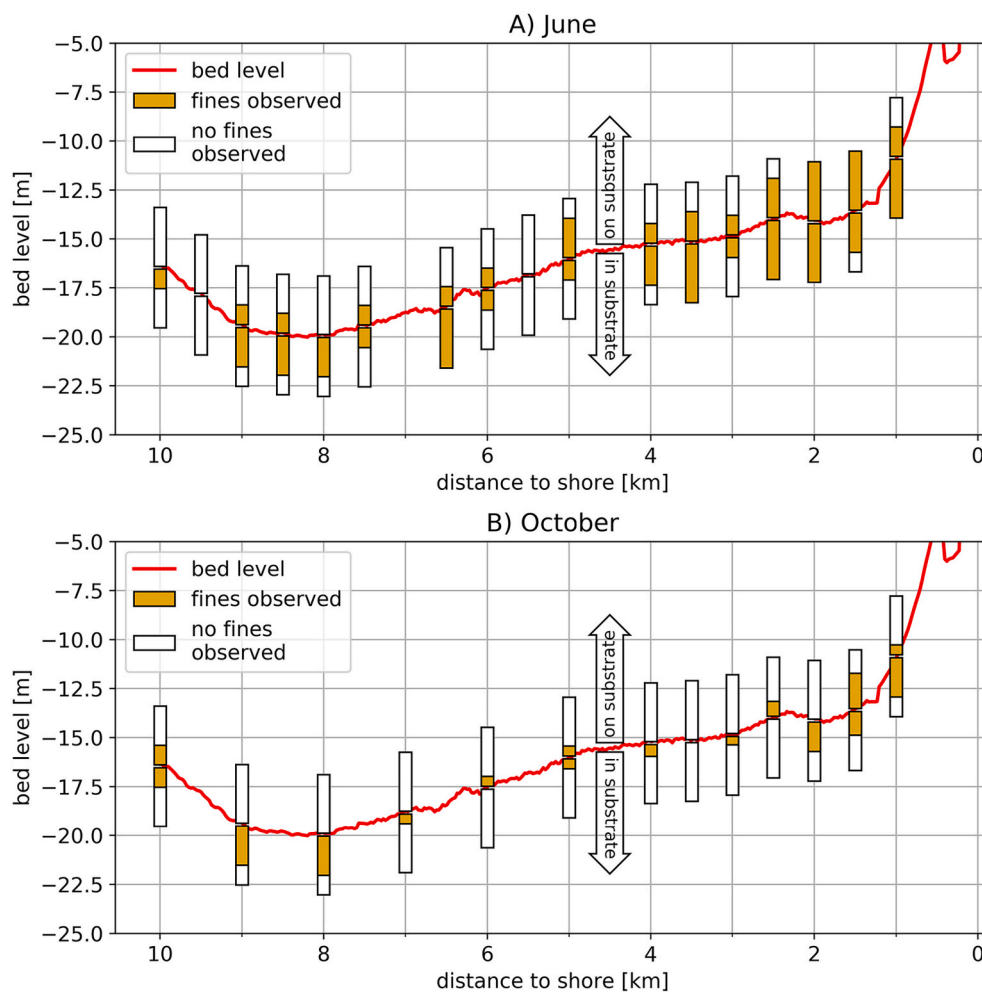

Fig. 12. A) fraction of SPI images with fines <u>on</u> and <u>in</u> substrate for June B) fraction of SPI images with fines <u>on</u> and <u>in</u> substrate for October.

5 km offshore (Fig. 12a), while they were much less frequently observed further offshore. For fines within the substrate, the same trend generally prevails, with the highest occurrences close to shore. The high fines percentages at 2 km offshore (Fig. 9a) are also reflected by the SPI images taken at that location.

4.4. Synthesis of data and conceptual model

In this section, the observations from both campaigns are compared to the conceptual model phases. For each sampling period, we determine to which phase of the dynamic cycle (cf. Fig. 3) the observations correspond and assess if the presence of fines (suspended, on or in the seabed) agrees with our hypotheses.

First, we consider the hydrodynamic conditions preceding and during the sampling period, as the four phases of the dynamic cycle are related to the occurrence of storms and transitions to and from calm conditions. We then establish the presence or absence of fines in the seabed. Next, we discuss the small-scale seabed morphology, i.e., whether the seabed is morphologically active or static during the measurement period. Both campaigns are first discussed separately. Then, both the spatial and temporal patterns are interpreted using the conceptual model.

4.4.1. June campaign

In June, sampling took place during a calm period, 3–4 days after a summer storm (Fig. 7c). Depending on the adjustment period after the storm, this should either be Phase 4 (post-storm) or Phase 1 (calm period) of the dynamic cycle. We can infer these phases from the bedform characteristics and fine sediment concentrations in both the water column and the seabed.

The small variations in bed elevation (Fig. 7e) at 4 km offshore suggest that the seabed was mostly morphologically static, and thus in Phase 1. This is confirmed by the relatively low SSC at this location (Fig. 7d). SSC showed a decreasing trend, but were low throughout the observation period. We would thus expect a limited exchange of fines between the seabed and water column as the majority of the fines would already have been buried. This is confirmed by the relatively high fines percentage in the seabed for most of the transect (Fig. 9a). Furthermore, fines are rarely observed on the substrate from 3 to 10 km offshore (Fig. 12a).

However, likely not the entire transect was in Phase 1. Within 2 km from the shore, the seabed was probably still in Phase 4. Here, the majority of SPI images showed fines both on and in the substrate, rather than solely within the substrate (Fig. 12a). The thick layer of fines on the substrate at 1.5 km offshore (Fig. 11 – right panel) is characteristic of Phase 4. Furthermore, bedforms higher than 2 cm were observed on SPI images at 2 and 1.5 km offshore.

The multiple seabed states are best illustrated by the SPI images shown in Fig. 11. The thick layer of fines on the substrate at 1.5 km offshore (Fig. 11 – right panel) is characteristic of Phase 4, while the SPI image collected 1 km further offshore clearly showed buried fines (Fig. 11 – left panel). As these images were collected within 30 min of each other, this suggests a variation in burial phase over larger distances (kilometres). Thus, the seabed can be in one phase closer to the shore, while in another phase further offshore.

4.4.2. October campaign

In October, measurements commenced shortly before a storm, while the seabed sampling took place during the storm peak and shortly post-storm (Fig. 8a, c). Hence, either Phase 3 or Phase 4 of the dynamic cycle (Fig. 3) is expected. The relatively large bedform height (Fig. 8f) and large variations thereof at 4 km offshore indeed suggest Phase 3. Furthermore, the near-bed SSC was high (Fig. 8d), while the fines percentages in the seabed were low (Fig. 9a).

Significant reconfiguration and migration of bedforms were recorded at 4 km offshore before seabed sampling took place. However, none of the sediment samples collected at 4 km offshore in October contained fines (Fig. 9a). This either means that Phase 3 of the dynamic cycle was still ongoing when the seabed was sampled, or that conditions in the post-storm period (Phase 4) were too energetic for fines to be buried at this location. Possibly, the swift decrease in bedform height shortly after the storm peak (Fig. 8f) prevented the burial of fines.

Moreover, the limited amount of burial in October is confirmed by sediment samples (Fig. 9c) and the SPI images (Fig. 12b). For the majority of the stations, hardly any fines were observed either on or in the substrate. Only the stations at larger water depths (at 6 and 8 km offshore) had considerable amounts of fines in the substrate. Moreover, at 6 km offshore, the SPI images and sediment samples are not entirely consistent as all sister samples at this station contained fines while this

was not observed in the SPI images.

4.4.3. Interpretation of spatial patterns

In June, measurements were collected during Phase 1 and 4, while in October measurements were collected during Phase 3 and 4 of our conceptual model. The observed presence of fines support the formulated hypothesis. We expected a strong vertical variation in, and patchy occurrences of, fines percentage in the seabed due to the burial process. This is confirmed by the sediment slices (Fig. 9b and c), which show fines in the seabed in distinct patches. Transitions from layers with fines to pure sand are abrupt, i.e., slices with a fines percentage of 4–5% are often adjacent to purely sandy slices. Fines are found both in isolated lenses and in adjacent slices. The latter are encountered either as larger patches of fines, or as successive layers of fines separated by thin layers of sand. In October, both were observed along the transect. At 8 km offshore, SPI images (not shown here, but available via the data repository) showed larger patches of fines, while at 6 km, images of the sediment cores exhibited successive layers of fines. Only the larger patches of fines may indicate another process than burial by small-scale bedforms. Both the abrupt transitions from fines to sand and successive layers of fines support the hypothesised burial process.

The presence of fines does not only vary vertically within the bed, but also horizontally. This is quantified through the variance in p_{fines} at three spatial scales, i.e. along the transect, per station and per sample (Fig. 13). For the entire transect, the mean fines percentage per station was used. For the stations, the mean fines percentage per sister sample was used, while per sample, it was the mean fines percentage per slice. The variance is of the same order of magnitude at all scales (Fig. 13). If fines were present, the variance within this sample sometimes even exceeded the variance along the entire transect, i.e. a larger vertical than horizontal variability.

This quantification agrees with qualitative observations from the SPI. These images (Fig. 10, Fig. 11) show how bed structure and the presence of fines vary significantly within 15 cm, which is the length of small-scale bedforms, i.e. decimetres. The variance within single stations is attributed to the variability in fines burial on megaripple scale (Phase 4 of the dynamic cycle – Fig. 3), since fines are only buried in the former trough of a megaripple and not under its former crest. Hence, the horizontal variation in fines percentages occurs within a metre (Fig. 9a), with significant variance.

4.4.4. Interpretation of temporal patterns

Another source of variability exists on the meso-scale. The approximate position on the shoreface determines if megaripples will form, owing to the combination of local hydrodynamic conditions and sediment characteristics. However, ripples and megaripples initially develop from small perturbations on the seabed, which are randomly distributed. Hence, the exact megaripple locations will also be randomly distributed. As net burial of fines only occurs in the trough of these megaripples, the presence of fines in the seabed inherits this stochastic behaviour. This may further explain the large variability in fines percentage over both decametres and hectometres. Interpretation of temporal patterns.

The observed sediment compositions are two snapshots in time and we cannot determine when the sampled sediment was actually deposited. However, we did observe a considerable change in fines percentages and distribution in the bed between June and October (Fig. 9a). As there are no indications that large-scale sedimentation or erosion took place between June and October, this implies that the fines present in the seabed in June were no longer there in October. Thus, they were remobilised from the bed between these two campaigns.

However, fines must still have been present in the seabed in the Egmond aan Zee area at the onset of the storm in October. Otherwise, the observed near-bed SSC at 4 km offshore (Fig. 8d) could not have increased up to 0.7 g/l within 1.5 day after the storm peak. However, if all the fines in the June samples at 4 km offshore would have been remobilised only during this single storm, this would have led to near-
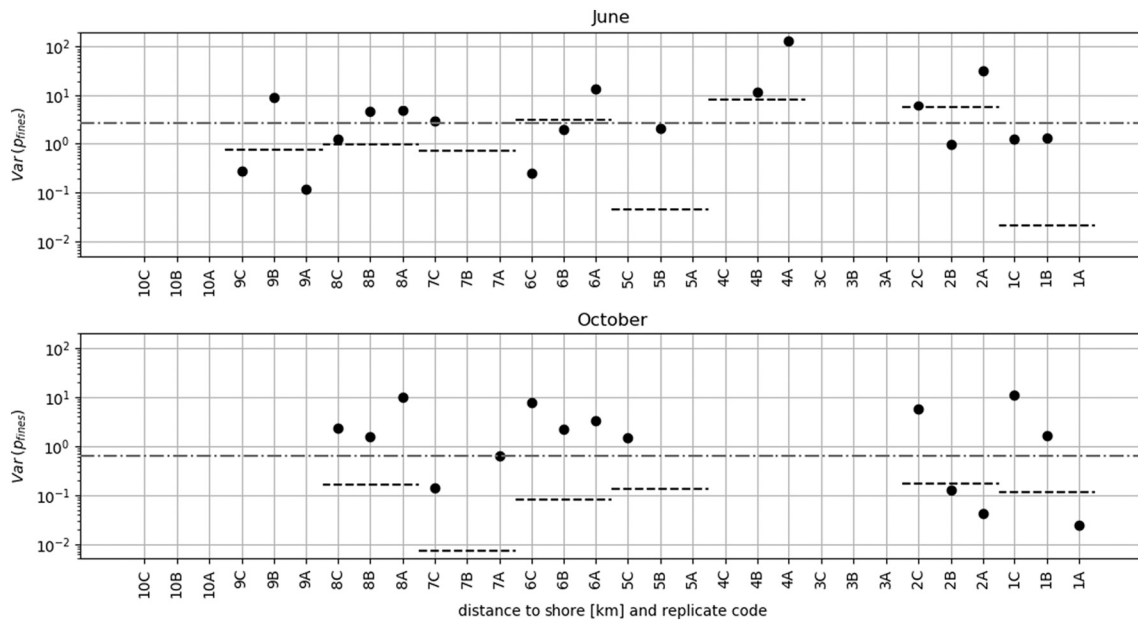
Fig. 13. Variance in fines percentage in June and October on three different spatial scales. (1) Grey dash-dot line: variance along the transect. (2) Black dashed lines: variance per station. (3) Black dots: variance per sediment sample.

bed SSC of >3 g/l. Thus, the majority of fines must have been remobilised prior to the October storm and advected away from the site. Hence, the data suggest that remobilisation of fines during storms can almost completely deplete the upper strata of a sandy seabed of fines. In that case, the SSC at this location is supply-limited through the limited availability of fines in the seabed.

5. Discussion

The field data collected in the southern North Sea corroborate the conceptual model with the dynamic burial cycle proposed therein. The presence of fines on and in the seabed varies considerably, both in time and space. In this section, we place our results into a wider perspective and discuss the implications of the hypothesised burial process for understanding fine sediment dynamics in shallow coastal seas.

5.1. Megaripple and ripple development and implications for burial

We argue that the interaction between wave-induced megaripples and tide-induced current ripples is essential for the burial of fines into a sandy seabed (see Fig. 3). During tide-dominated conditions, only current-induced ripples are found on the seabed. These bury and release fines during their migration, but are not expected to contribute to net burial after their initial capture, nor are they expected to bury fines at larger depths. Net burial only takes place in the wake of storms, when megaripples formed during the storm gradually adjust, flattening and reforming into current-induced ripples. Hence, in order to understand where and when burial of fines takes place, understanding the formation and subsequent flattening of megaripples is crucial.

When a storm occurs, bedform height and length swiftly adjust to governing conditions. The maximum megaripple length, height, and associated timescale depend on the wave-induced Shields parameter ($\theta_w = \frac{\tau_w}{\rho(s-1)gd_{50}}$) (Soulsby et al., 2012; Traykovski, 2007), thus on the wave-induced bed shear stress and d_{50}. As this shear stress increases quadratically with decreasing water depth, θ_w strongly varies in both space and time in the southern North Sea (Brakenhoff et al., 2020; Wengrove et al., 2018). On the ebb-tidal delta of Ameland, for instance, θ_w varies by three orders of magnitude within several kilometres during a one month period, from 10^{-3} to 10^0 (Brakenhoff et al., 2020). Hence,

the critical Shields parameter for fine sand ($\theta_{cr} \approx 5*10^{-3}$) is not exceeded in some areas while in others, sheet flow can occur ($\theta_{sh} \approx 10^0$). On the lower shoreface of the southern North Sea, where bathymetric gradients are less pronounced than on ebb-tidal deltas, differences in θ_w are still considerable over larger areas, with reported values ranging from $2*10^{-3}$ to 10^0 (Passchier and Kleinhans, 2005; van der Werf et al., 2022).

The timescale associated with the flattening of wave-induced megaripples to current-induced ripples (T_r) dictates the period during which deep burial can occur. It depends on the megaripple dimensions formed during storms and the current-induced Shields parameter θ_c. The latter depends on tidal flow velocity and d_{50}. Tidal flow velocities vary over multiple timescales (e.g., diurnal and fortnightly, spring-neap) and in space. Variations in θ_c are generally smaller than θ_w, with values for the lower shoreface of the southern North Sea ranging from $2*10^{-3}$ to $2*10^{-1}$ (Passchier and Kleinhans, 2005; van de Meene and van Rijn, 2000). Moreover, their magnitude decreases in onshore direction (Kleinhans and Grasmeijer, 2006).

To illustrate this timescale for deep burial, we sketched how bedform height (η) develops during and after a storm (Fig. 14a). Before the storm, only tide-induced current ripples with height η_c are found. A storm takes place, and megaripples with height η_{storm} are formed. Three potential pathways are sketched (dashed lines in Fig. 14a), each having a different ratio between θ_c and the critical Shields parameter θ_{cr}. These are: (I) no change in bedform height as the tidal current is too weak to mobilise sand ($\theta_c < \theta_{cr}$), (II) a strong decrease ($\theta_c >> \theta_{cr}$) and (III) a gradual decrease ($\theta_c \approx \theta_{cr}$). For each path, the timescale is indicated by $T_{r,n}$.

The first path (I) represents calm post-storm conditions. Hence, fines accumulate in the troughs of the bedforms, atop the seabed. However, no burial takes place as there are no migrating ripples. The associated timescale $T_{r,I}$ is thus (theoretically) infinitely large. Along the second path, megaripples reconfigure swiftly to the post-storm conditions, $T_{r,II}$ is small, leaving little time for deposition of fines in the megaripple troughs. Hence, burial is probably limited. Along the third path, megaripples flatten out gradually, with an associated timescale of several days ($T_{r,III}$). Fines may settle atop the seabed during several successive slack tides and are subsequently buried into the seabed.

These examples imply that if tidal currents are too small or too large, little to no burial takes place. Optimal burial efficiency is likely found somewhere in between at moderate tidal currents. We conceptualised
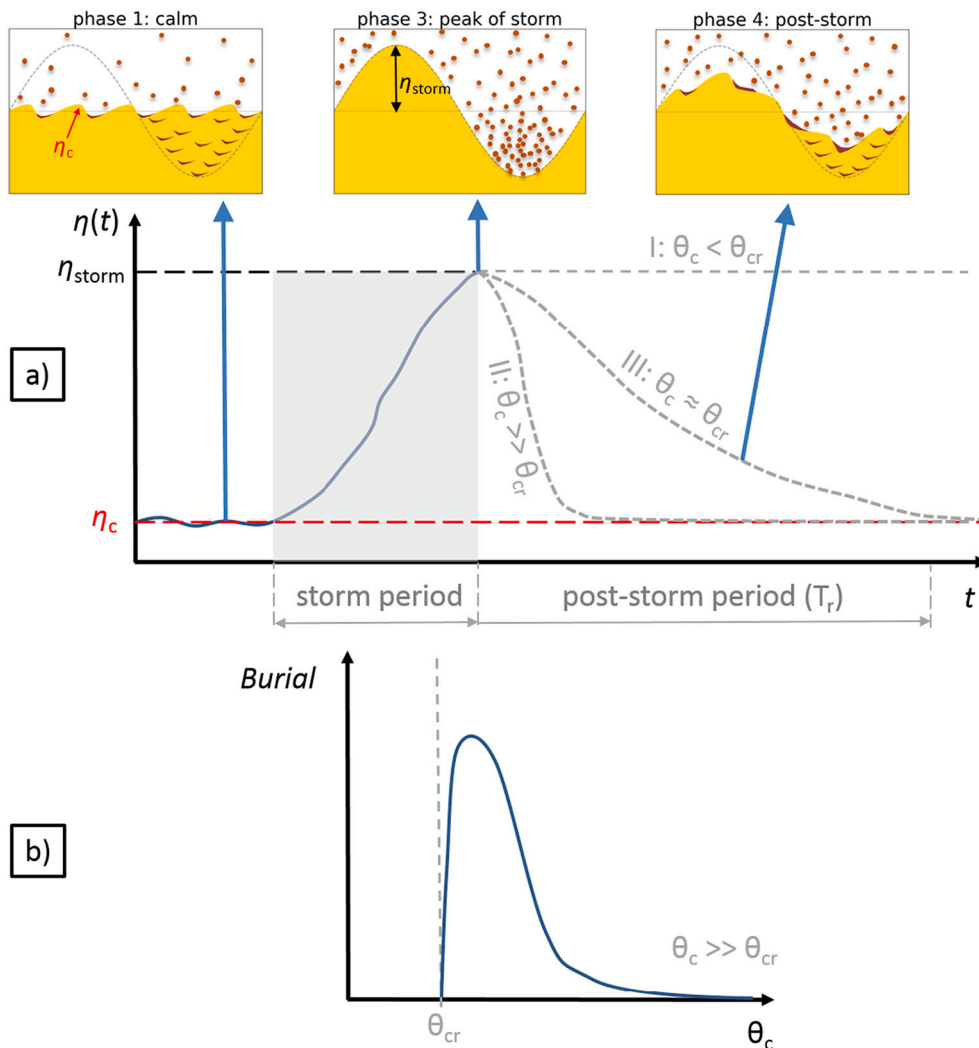
Fig. 14. a) Conceptual sketch of bedform height during and after a storm, showing different possible paths determining burial efficiency. b) Hypothetical relationship between burial rate and θ_c.

this argument through the relationship between burial and θ_c in Fig. 14b. This provides a possible way forward for modelling and parameterising the burial of fines in the seabed of coastal shelf seas.

Parameterisations which aggregate the burial process on larger spatial and temporal scales are required, as hydro- and morphodynamic models typically operate on length scales of one to several orders of magnitude larger than the proposed burial process. Hence, these parameterisations should aim at correctly representing large-scale patterns of fines in the seabed, and consider the temporal and spatial variations of wave and current bed shear stress. However, this is beyond the scope of the present paper. For upscaling and validating the conceptual model on a regional level, we advise to study seabed dynamics in detail on other sites in the southern North Sea. Collecting multibeam bathymetry and backscatter with sufficient resolution seems crucial to validate the occurrence of (mega-) ripples (Koop et al., 2020). The mobility of small-scale ripples is of interest and may be validated by using instrumented landers.

5.2. Spatial variability in presence of fines

We have combined the conceptual model and observations to explain why fines presence varies on a small scale, down to metres or decimetres. In this model, seabed structure has been simplified to bi-modal conditions, i.e., indicating the presence or absence of fines. Seabed data

have been simplified using similar classifications (Fig. 9, Fig. 12). In reality, the surficial seabed and underlying strata are often more complex than a bi-modal classification would suggest. Geological deposits, benthic species, (remnants of) shells can all be found in the upper seabed strata (van der Spek et al., 2020). These other elements can be considered passive, not disturbing the burial process, for a seabed that is predominantly made up of sand and fines. The formation and migration of bedforms is disturbed if such elements are abundantly present, e.g., as erosion-resistant layers (e.g. peat or stiff clay) (Passchier and Kleinhans, 2005) or by abundant presence of shell fragments (Cheng et al., 2021).

For the Egmond aan Zee transect, this bi-modal classification seems justified. The SPI yielded valuable information on seabed structure, which is often lost when sampling it (van Hoey et al., 2004). The SPI images show a bed which primarily consists of sand with distinct patches of fines. Quantification of the seabed structure from the SPI observations was possible as fines were present in patches with a distinct colour and texture compared to other seabed features (Fig. 12). Further validation of this approach with quantitative methods (e.g. grain size distribution) is recommended.

There is not only a variability in fines presence on the small-scale but also on hectometre-kilometre scale (Hendriks et al., 2020; van Alphen, 1987b). On these larger scales, the presence of fines in and on the seabed is governed by a combination of three factors: (1) sources of fines, (2) transport pathways and (3) accumulation potential. The latter is

determined by a combination of current-induced bed shear stress and seabed topography (Hendriks et al., 2020). Whether fines are actually buried in the seabed after deposition depends on the local burial process.

The variability in fines presence on both large and small scale makes it virtually impossible to predict the exact fines percentage in the upper seabed strata at a certain location. Statistical approaches to estimate the probability of encountering fines in the seabed seem more valuable, either by geostatistical approaches (Bockelmann et al., 2018; Stephens and Diesing, 2015) or physics-based classifications (Hendriks et al., 2020).

5.3. Temporal variability in presence of fines

When fines are regularly exchanged with the seabed, the water column and seabed must be analysed as a coupled system. Fines presence in the seabed depends on deposition of fines from the water column and subsequent burial. Vice versa, suspended sediment concentrations cannot be understood by only considering processes taking place in the water column.

The presence of fines in the seabed depends on a succession of storms and subsequent calm conditions over the course of months to years. This dependency leads to substantial memory effects, as the individual storms determine how much fines can be buried at which depth. On the short term, the storm's magnitude determines how long the seabed remains affected by that particular storm. Wave-induced megaripples become longer and higher when storms are more intense, leading to a potential deeper burial of fines. Without significant reworking of the sediment by biota, it would require a storm of similar magnitude to remobilise the previously buried fines. The larger a storm, the longer it takes for a similar storm occurs. Hence, some fines are then buried deep for long periods. For weekly to monthly timescales, the burial depths are thus on the order of 10–20 cm, corresponding to megaripple heights formed during a single storm. On longer timescales, on the order of years to decades, burial depths of 30 cm (Laane et al., 1999) are probable. On these timescales, the active layer, and thus burial depth, may even be up to 50–60 cm as long-term shoreface erosion and migration or reconfiguration of larger geomorphological features start to play a role (van der Spek et al., 2022, 2020).

In the water column, SSC magnitude depends on local fine sediment availability (Eleveld et al., 2008; Flores et al., 2017; Stanev et al., 2009; Suijlen and Duin, 2001; van der Hout et al., 2017). This availability is determined by storms, which remobilise fines that were previously buried within the seabed. Once fines have been remobilised, SSC varies on diurnal and fortnightly timescales (McCandliss et al., 2002; Stanev et al., 2009; van der Hout et al., 2017). Though, their magnitude differs substantially before and after storms. Under similar hydrodynamic forcing, SSC may be up to an order of magnitude higher after storms than before (Flores et al., 2017). How long a storm affects SSC depends on how effectively fines are buried within the seabed after a storm (Fig. 14). This memory in the system should be considered when interpreting SSC time series, meaning that observed SSC cannot be interpreted as an instantaneous response to prevailing hydrodynamic forcing (Stanev et al., 2009; van der Hout et al., 2017).

6. Conclusions

In this study, we have shown how small-scale bedforms can bury fines in the sandy seabed of the southern North Sea. We developed a mechanistic description of the process, using field data collected in the southern North Sea to develop and test this model.

The burial process consists of four distinct phases forming a dynamic cycle. These phases are related to the occurrence of storms. Fines remobilised during storms will subsequently settle and deposit on top of a sandy seabed. Interactions between bedforms of different scales are then crucial to bury fines in the seabed. Megaripples formed during storms gradually adjust to calmer conditions in the wake of storms.

During this adjustment period, fines are buried by current-induced ripples in the troughs of the former megaripples. Thus, fines can be buried in the seabed at depths of up to 10–15 cm. This burial process affects the presence of fines in the bed, both in time and space. The observed temporal variation in fines percentage implies that the seabed is occasionally depleted of fines, resulting in supply-limited conditions. Furthermore, fines percentages in the seabed vary considerably on multiple spatial scales. They both vary on the mega-scale (kilometres) and on the micro-scale (metres-centimetres). Fines are found in distinct patches, both horizontally and vertically. The micro-scale is multiple orders of magnitude smaller than the scale on which hydromorphological models operate. This means that small-scale variations in monitoring data cannot be reflected in a numerical model outcome. Model parameterisations are needed to aggregate the effects of burial on larger spatial scales.

Moreover, the effectivity and associated timescale for burial depend on the ratio between storm intensity and current magnitude. Theoretically, this leads to an optimum in burial conditions. If tidal currents are too small, sand is not mobilised and no burial takes place. For large tidal currents, the time window for burial is short and likely results in limited burial. Hence, an optimum burial condition is found somewhere in between.

This study provides a basis for mechanistic model parameterisations of fines burial into a sandy seabed. These are required, since fine sediment dynamics strongly depend on the exchange of fines with the sandy seabed. As suspended fine sediments affect the ecological functioning of shallow coastal seas, a better understanding of these dynamics will prove crucial in conserving these vital ecosystems under increasing anthropogenic pressure.

Data statement

The data that support the findings of this study are openly available in standardised formats through the 4TU.ResearchData repository at https://doi.org/10.4121/c.6001987.

Declaration of Competing Interest

The authors declare that they have no known competing financial interests or personal relationships that could have appeared to influence the work reported in this paper.

Acknowledgements

References

Amos, C.L., Li, M.Z., Choung, K.S., 1996. Storm-generated, hummocky stratification on the outer-Scotian Shelf. Geo-Mar. Lett. 16, 85–94. https://doi.org/10.1007/BF02202602.

Amos, C.L., Bowen, A.J., Huntley, D.A., Judge, J.T., Li, M.Z., 1999. Ripple migration and sand transport under quasi-orthogonal combined flows on the Scotian Shelf. J. Coast. Res. 15, 1–14.

Anthony, E.J., Aagaard, T., 2020. The lower shoreface: morphodynamics and sediment connectivity with the upper shoreface and beach. Earth-Sci. Rev. 210 https://doi.org/10.1016/j.earscirev.2020.103334.

Anthony, K.R.N., Ridd, P.V., Orpin, A.R., Larcombe, P., Lough, J., 2004. Temporal variation of light availability in coastal benthic habitats: effects of clouds, turbidity,

and tides. Limnol. Oceanogr. 49, 2201–2211. https://doi.org/10.4319/lo.2004.49.6.2201.

Baas, J.H., van Dam, R.L., Storms, J.E.A., 2000. Duration of deposition from decelerating high-density turbidity currents. Sediment. Geol. 136, 71–88. https://doi.org/10.1016/S0037-0738(00)00088-9.

Bockelmann, F.D., Puls, W., Kleeberg, U., Müller, D., Emeis, K.C., 2018. Mapping mud content and median grain-size of North Sea sediments – a geostatistical approach. Mar. Geol. 397, 60–71. https://doi.org/10.1016/j.margeo.2017.11.003.

Brakenhoff, L., Kleinhans, M., Ruessink, G., van der Vegt, M., 2020. Spatio-temporal characteristics of small-scale wave–current ripples on the Ameland ebb-tidal delta. Earth Surf. Process. Landforms 45, 1248–1261. https://doi.org/10.1002/esp.4802.

Breton, S.-P., Moe, G., 2009. Status, plans and technologies for offshore wind turbines in Europe and North America. Renew. Energy 34, 646–654. https://doi.org/10.1016/J.RENENE.2008.05.040.

Callesen, I., Keck, H., Andersen, T.J., 2018. Particle size distribution in soils and marine sediments by laser diffraction using Malvern Mastersizer 2000—method uncertainty including the effect of hydrogen peroxide pretreatment. J. Soils Sediments 18, 2500–2510. https://doi.org/10.1007/s11368-018-1965-8.

Cheng, C.H., Soetaert, K., Borsje, B.W., 2020. Sediment characteristics over asymmetrical tidal sand waves in the Dutch north sea. J. Mar. Sci. Eng. 8 https://doi.org/10.3390/JMSE8060409.

Cheng, C.H., de Smit, J.C., Fivash, G.S., Hulscher, S.J.M.H., Borsje, B.W., Soetaert, K., 2021. Sediment shell-content diminishes current-driven sand ripple development and migration. Earth Surf. Dyn. 9, 1335–1346. https://doi.org/10.5194/ESURF-9-1335-2021.

Colosimo, I., de Vet, P.L.M., van Maren, D.S., Reniers, A.J.H.M., Winterwerp, J.C., van Prooijen, B.C., 2020. The impact of wind on flow and sediment transport over intertidal flats. J. Mar. Sci. Eng. 8, 1–26. https://doi.org/10.3390/jmse8110910.

Damen, J.M., van Dijk, T.A.G.P., Hulscher, S.J.M.H., 2018. Spatially varying environmental properties controlling observed sandwave morphology. J. Geophys. Res. Earth Surf. 123, 983–1008. https://doi.org/10.1002/2014JF003418.Received.

Dankers, P.J.T., 2005. The Intrusion of Fine Suspended Sediment into a Sandy Sediment Bed. A Literature Review. Delft, The Netherlands.

de Boer, G.J., Pietrzak, J.D., Winterwerp, J.C., 2009. SST observations of upwelling induced by tidal straining in the Rhine ROFI. Cont. Shelf Res. 29, 263–277. https://doi.org/10.1016/j.csr.2007.06.011.

Degraer, S., Van Lancker, V., Van Dijk, T.A.G.P., Birchenough, S.N.R., De Witte, B., Elliott, M., Le Bot, S., Reiss, H., Stelzenmüller, V., Van Gaever, S., Balian, E., Cox, D., Hernandez, F., Lacroix, G., Lindeboom, H., Reubens, J., Soetaert, K., 2019. Interdisciplinary science to support North Sea marine management: lessons learned and future demands. Hydrobiol. Special Isuse 1–11. https://doi.org/10.1007/s10750-019-04109-9.

Eisma, D., 1968. Composition, Origin and Distribution of Dutch Coastal Sands between Hoek Van Holland and the Island of Vlieland. E.J. Brill.

Eleveld, M.A., Pasterkamp, R., van der Woerd, H.J., Pietrzak, J.D., 2008. Remotely sensed seasonality in the spatial distribution of sea-surface suspended particulate matter in the southern North Sea. Estuar. Coast. Shelf Sci. 80, 103–113. https://doi.org/10.1016/j.ecss.2008.07.015.

Elgar, S., Raubenheimer, B., Guza, R., 2005. Quality control of acoustic Doppler velocimeter data in the surfzone. Meas. Sci. Technol. 16, 1889. https://doi.org/10.1088/0957-0233/16/10/002.

Fernandez, R., Best, J., López, J., 2006. Mean flow, turbulence structure, and bed form superimposition across the ripple-dune transition. Water Resour. Res. 42, 1–17. https://doi.org/10.1029/2005WR004330.

Fettweis, M., van den Eynde, D., 2003. The mud deposits and the high turbidity in the Belgian-Dutch coastal zone, southern bight of the North Sea. Cont. Shelf Res. 23, 669–691. https://doi.org/10.1016/S0278-4343(03)00027-X.

Fettweis, M., Francken, F., van den Eynde, D., Verwaest, T., Janssens, J., van Lancker, V., 2010. Storm influence on SPM concentrations in a coastal turbidity maximum area with high anthropogenic impact (southern North Sea). Cont. Shelf Res. 30, 1417–1427. https://doi.org/10.1016/J.CSR.2010.05.001.

Fettweis, M., Monbaliu, J., Baeye, M., Nechad, B., Van den Eynde, D., 2012. Weather and climate induced spatial variability of surface suspended particulate matter concentration in the North Sea and the English Channel. Methods Oceanogr. 3–4, 25–39. https://doi.org/10.1016/j.mio.2012.11.001.

Fettweis, M., Riethmüller, R., Verney, R., Becker, M., Backers, J., Baeye, M., Chapalain, M., Claeys, S., Claus, J., Cox, T., Deloffre, J., Depreiter, D., Druine, F., Flöser, G., Grünler, S., Jourdin, F., Lafite, R., Nauw, J., Nechad, B., Röttgers, R., Sottolichio, A., van Engeland, T., Vanhaverbeke, W., Vereecken, H., 2019. Uncertainties associated with in situ high-frequency long-term observations of suspended particulate matter concentration using optical and acoustic sensors. Prog. Oceanogr. 178, 102162 https://doi.org/10.1016/j.pocean.2019.102162.

Flores, R.P., Rijnsburger, S., Horner-Devine, A.R., Souza, A.J., Pietrzak, J.D., 2017. The impact of storms and stratification on sediment transport in the Rhine region of freshwater influence. J. Geophys. Res. Ocean. 122 https://doi.org/10.1002/2014JC010066.Received.

Germano, J.D., Rhoads, D.C., Valente, R.M., Carey, D.a., Solan, M., 2011. The use of Sediment Profile Imaging (SPI) for environmental impact assessments and monitoring studies: lessons learned from the past four decades. Oceanogr. Mar. Biol. Annu. Rev. 49, 235–298. https://doi.org/10.1201/b11009.

Goring, D., Nikora, V., 2002. Despiking acoustic doppler velocimeter data. J. Hydraul. Eng. - ASCE 128. https://doi.org/10.1061/(ASCE)0733-9429(2002)128:1(117.

Graf, G., Rosenberg, R., 1997. Bioresuspension and biodeposition: a review. J. Mar. Syst. 11, 269–278. https://doi.org/10.1016/S0924-7963(96)00126-1.

Grasmeijer, B., Huisman, B., Luijendijk, A., Schrijvershof, R., van der Werf, J., Zijl, F., de Looff, H., de Vries, W., 2022. Modelling of annual sand transports at the Dutch lower

shoreface. Ocean Coast. Manag. 217, 105984 https://doi.org/10.1016/J.OCECOAMAN.2021.105984.

Harrison, W.D., Musgrave, D., Reeburgh, W.S., 1983. A wave-induced transport process in marine sediments. J. Geophys. Res. 88, 7617. https://doi.org/10.1029/JC088iC12p07617.

Hendriks, H.C.M., van Prooijen, B.C., Aarninkhof, S.G.J., Winterwerp, J.C., 2020. How human activities affect the fine sediment distribution in the Dutch Coastal Zone seabed. Geomorphology 367, 107314. https://doi.org/10.1016/j.geomorph.2020.107314.

Houthuys, R., Trentesaux, A., De Wolf, P., 1994. Storm influences on a tidal sandbank's surface (Middelkerke Bank, southern North Sea). Mar. Geol. 121, 23–41.

Huettel, M., Rusch, A., 2000. Transport and degradation of phytoplankton in permeable sediment. Limnol. Oceanogr. 45, 534–549. https://doi.org/10.4319/lo.2000.45.3.0534.

Huettel, M., Ziebis, W., Forster, S., 1996. Flow-induced uptake of particulate matter in permeable sediments. Limnol. Oceanogr. 41, 309–322. https://doi.org/10.4319/lo.1996.41.2.0309.

Hulscher, S.J.M.H., van den Brink, G.M., 2001. Comparison between predicted and observed sand waves and sand banks in the North Sea. J. Geophys. Res. 106, 9327. https://doi.org/10.1029/2001JC900003.

Hunter, J.D., 2007. Matplotlib: a 2D graphics environment. Comput. Sci. Eng. 9, 90–95. https://doi.org/10.1109/MCSE.2007.55.

Jennes, M., Duineveld, G.C.A., 1985. Effects of tidal currents on chlorophyll a content of sandy sediments in the southern North Sea. Mar. Ecol. Prog. Ser. 21, 283–287. https://doi.org/10.3354/meps021283.

Karakassis, I., Tsapakis, M., Smith, C.J., Rumohr, H., 2002. Fish farming impacts in the Mediterranean studied through sediment profiling imagery. Mar. Ecol. Prog. Ser. 227, 125–133. https://doi.org/10.3354/meps227125.

Kirk, J.T.O., 1994. Light and Photosynthesis in Aquatic Ecosystems. Cambridge University Press, Cambridge. https://doi.org/10.1017/CBO9780511623370.

Kleinhans, M.G., Grasmeijer, B.T., 2006. Bed load transport on the shoreface by currents and waves. Coast. Eng. 53, 983–996. https://doi.org/10.1016/J.COASTALENG.2006.06.009.

Kleinhans, M.G., Montfort, O., Dankers, P.J.T., Van Rijn, L.C., Bonne, W., 2005. Mud dynamics on the shoreface and upper shelf, {Noordwijk, the Netherlands}. Sandpit Proj. 5, Q1–Q16.

Koop, L., van der Reijden, K.J., Mestdagh, S., Ysebaert, T., Govers, L.L., Olff, H., Herman, P.M.J., Snellen, M., Simons, D.G., 2020. Measuring centimeter-scale sand ripples using multibeam echosounder backscatter data from the brown bank area of the Dutch Continental Shelf. Geosci. 2020 10, 495. https://doi.org/10.3390/GEOSCIENCES10120495.

Kristensen, E., Penha-Lopes, G., Delefosse, M., Valdemarsen, T., Quintana, C.O., Banta, G. T., 2012. What is bioturbation? The need for a precise definition for fauna in aquatic sciences. Mar. Ecol. Prog. Ser. 446, 285–302. https://doi.org/10.3354/MEPS09506.

Laane, R.W.P.M., Sonneveldt, H.L.A., Van Der Weyden, A.J., Loch, J.P.G., Groeneveld, G., 1999. Trends in the spatial and temporal distribution of metals (Cd, Cu, Zn and Pb) and organic compounds (PCBs and PAHs) in Dutch coastal zone sediments from 1981 to 1996: a model case study for Cd and PCBs. J. Sea Res. 41, 1–17. https://doi.org/10.1016/S1385-1101(98)00038-0.

Le Hir, P., Monbet, Y., Orvain, F., 2007. Sediment erodability in sediment transport modelling: can we account for biota effects? Cont. Shelf Res. 27, 1116–1142. https://doi.org/10.1016/j.csr.2005.11.016.

Lecroart, P., Schmidt, S., Anschutz, P., Jouanneau, J.M., 2007. Modeling sensitivity of biodiffusion coefficient to seasonal bioturbation. J. Mar. Res. 65, 417–440. https://doi.org/10.1357/002224007781567630.

Li, M.Z., Amos, C.L., 1999. Field observations of bedforms and sediment transport thresholds of fine sand under combined waves and currents. Mar. Geol. 158, 147–160. https://doi.org/10.1016/S0025-3227(98)00166-2.

Lichtman, I.D., Baas, J.H., Amoudry, L.O., Thorne, P.D., Malarkey, J., Hope, J.A., Peakall, J., Paterson, D.M., Bass, S.J., Cooke, R.D., Manning, A.J., Davies, A.G., Parsons, D.R., Ye, L., 2018. Bedform migration in a mixed sand and cohesive clay intertidal environment and implications for bed material transport predictions. Geomorphology 315, 17–32. https://doi.org/10.1016/j.geomorph.2018.04.016.

Marten, K.V., 2010. Field Observation and Modelling of Near-Shore Sediment Transport Processes. Bangor University, UK.

Martin, A.J., 2000. Flaser and wavy bedding in ephemeral streams: a modern and an ancient example. Sediment. Geol. 136, 1–5. https://doi.org/10.1016/S0037-0738(00)00085-3.

Martinius, A.W., van den Berg, J.H., 2011. Atlas of Sedimentary Structures in Estuarine and Tidally-Influenced River Deposits of the Rhine-Meuse-Scheldt System: Their Application to the Interpretation of Analogous Outcrop and Subsurface Depositional Systems, 1st ed. EAGE Publications BV, Houten, the Netherlands.

McCandliss, R.R., Jones, S.E., Hearn, M., Latter, R., Jago, C.F., 2002. Dynamics of suspended particles in coastal waters (southern North Sea) during a spring bloom. J. Sea Res. 47, 285–302. https://doi.org/10.1016/S1385-1101(02)00123-5.

McCave, I.N., Bryant, R.J., Cook, H.F., Coughanowr, C.A., 1986. Evaluation of a laser-diffraction-size analyzer for use with natural sediments. J. Sediment. Res. 56, 561–564. https://doi.org/10.1306/212F89CC-2B24-11D7-8648000102C1865D.

McLean, S.R., Nelson, J.M., Wolfe, S.R., 1994. Turbulence structure over two-dimensional bed forms: implications for sediment transport. J. Geophys. Res. 99, 12729. https://doi.org/10.1029/94JC00571.

Meirelles, S., Henriquez, M., Souza, A.J., Horner-Devine, A.R., Pietrzak, J.D., Rijnsburg, S., Stive, M.J.F., 2016. Small scale bedform types off the South-Holland Coast. J. Coast. Res. 1, 423–426. https://doi.org/10.2112/SI75-085.1/29687/SMALL-SCALE-BEDFORM-TYPES-OFF-THE-SOUTH-HOLLAND.

Middelburg, J.J., Soetaert, K., Herman, P.M.J., 1997. Empirical relationships for use in global diagenetic models. Deep Sea Res. Part I Oceanogr. Res. Pap. 44, 327–344. https://doi.org/10.1016/S0967-0637(96)00101-X.

NLHO, Deltares, 2019. Netherlands Hydrographic Office bathymetric data [WWW Document]. http://opendap.deltares.nl/thredds/catalog/opendap/hydrografie/catalog.html.

Passchier, S., Kleinhans, M.G., 2005. Observations of sand waves, megaripples, and hummocks in the Dutch coastal area and their relation to currents and combined flow conditions. J. Geophys. Res. Earth Surf. 110 https://doi.org/10.1029/2004JF000215.

Piet, G., Culhane, F., Jongbloed, R., Robinson, L., Rumes, B., Tamis, J., 2019. An integrated risk-based assessment of the North Sea to guide ecosystem-based management. Sci. Total Environ. 654, 694–704. https://doi.org/10.1016/J.SCITOTENV.2018.11.001.

Pietrzak, J.D., de Boer, G.J., Eleveld, M.A., 2011. Mechanisms controlling the intra-annual mesoscale variability of SST and SPM in the southern North Sea. Cont. Shelf Res. 31, 594–610. https://doi.org/10.1016/J.CSR.2010.12.014.

Reineck, H.-E., Singh, I.B., 1980. Depositional Sedimentary Environments with Reference to Terrigenous Clastics, 2nd ed. Springer Berlin, Heidelberg, Germany.

Reineck, H.E., Wunderlich, F., 1968. Classification and origin of flaser and lenticular bedding. Sedimentology 11, 99–104. https://doi.org/10.1111/j.1365-3091.1968.tb00843.x.

Rhoads, D., Germano, J., 1982. Characterization of organism-sediment relations using sediment profile imaging: an efficient method of remote ecological monitoring of the seafloor (Remots™ System). Mar. Ecol. Prog. Ser. 8, 115–128. https://doi.org/10.3354/meps008115.

Rijnsburger, S., van der Hout, C.M., van Tongeren, O., de Boer, G.J., van Prooijen, B.C., Borst, W.G., Pietrzak, J.D., 2016. Simultaneous measurements of tidal straining and advection at two parallel transects far downstream in the Rhine ROFI. Ocean Dyn. 66, 719–736. https://doi.org/10.1007/s10236-016-0947-x.

Rijnsdorp, A., Poos, J.J., Quirijns, F.J., HilleRisLambers, R., De Wilde, J.W., Den Heijer, W.M., 2008. The arms race between fishers. J. Sea Res. 60, 126–138. https://doi.org/10.1016/J.SEARES.2008.03.003.

Romero-Ramirez, A., Grémare, A., Desmalades, M., Duchêne, J.C., 2013. Semi-automatic analysis and interpretation of sediment profile images. Environ. Model. Softw. 47, 42–54. https://doi.org/10.1016/j.envsoft.2013.04.008.

Sanford, L.P., 2008. Modeling a dynamically varying mixed sediment bed with erosion, deposition, bioturbation, consolidation, and armoring. Comput. Geosci. 34, 1263–1283. https://doi.org/10.1016/j.cageo.2008.02.011.

Schrijvershof, R., Brakenhoff, L., Grasmeijer, B., 2019. Hydrodynamics and Bedforms on the Dutch Lower Shoreface. Delft, The Netherlands.

Soulsby, R.L., Whitehouse, R.J.S., Marten, K.V., 2012. Prediction of time-evolving sand ripples in shelf seas. Cont. Shelf Res. 38, 47–62. https://doi.org/10.1016/j.csr.2012.02.016.

Stanev, E.V., Dobrynin, M., Pleskachevsky, A., Grayek, S., Günther, H., 2009. Bed shear stress in the southern North Sea as an important driver for suspended sediment dynamics. Ocean Dyn. 59, 183–194. https://doi.org/10.1007/s10236-008-0171-4.

Stephens, D., Diesing, M., 2015. Towards quantitative spatial models of seabed sediment composition. PLoS One 10, 1–23. https://doi.org/10.1371/journal.pone.0142502.

Stolk, A., Dijkshoorn, C., 2009. Sand extraction Maasvlakte 2 Project: License, Environmental Impact Assessment and Monitoring. In: Eur. Mar. Sand Gravel Gr. - a wave Oppor. Mar. aggregates Ind. EMSAGG Conf. 7–8 May 2009.

Suijlen, J.M., Duin, R.N.M., 2001. Variability of near-Surface Total Suspended Matter Concentrations in the Dutch Coastal Zone of the North Sea. The Hague, The Netherlands.

Tanaka, H., Van Dang, T., 1996. Geometry of sand ripples due to combined wave-current flows. J. Waterw. Port Coast. Ocean Eng. 122, 298–3000. https://doi.org/10.1061/(ASCE)0733-950X(1996)122:6(298).

Terwindt, J.H.J., Breusers, H.N.C., 1972. Experiments on the origin of flaser, lenticular and sand-clay alternating bedding. Sedimentology 19, 85–98. https://doi.org/10.1111/j.1365-3091.1972.tb00237.x.

Traykovski, P., 2007. Observations of wave orbital scale ripples and a nonequilibrium time-dependent model. J. Geophys. Res. Ocean. 112, 1–19. https://doi.org/10.1029/2006JC003811.

Traykovski, P., Hay, A.E., Irish, J.D., Lynch, J.F., 1999. Geometry, migration, and evolution of wave orbital ripples at LEO-15. J. Geophys. Res. Ocean. 104, 1505–1524. https://doi.org/10.1029/1998jc900026.

van Alphen, J.S.L.J., 1987a. Slibvoorkomens op het Nederlands en Belgisch deel van het Continentaal Plat. Rijswijk, The Netherlands.

van Alphen, J.S.L.J., 1987b. Slibvoorkomens landwaarts 10m lijn tussen Terheijde en Noordwijk. Rijswijk, The Netherlands.

van Alphen, J.S.L.J., 1990. A mud balance for Belgian-Dutch coastal waters between 1969 and 1986. Netherlands J. Sea Res. 25, 19–30. https://doi.org/10.1016/0077-7579(90)90005-2.

van de Meene, J.W.H., van Rijn, L.C., 2000. The shoreface-connected ridges along the central Dutch coast - part 1: Field observations. Cont. Shelf Res. 20, 2295–2323. https://doi.org/10.1016/S0278-4343(00)00048-0.

van der Hout, C.M., Gerkema, T., Nauw, J.J., Ridderinkhof, H., 2015. Observations of a narrow zone of high suspended particulate matter (SPM) concentrations along the Dutch coast. Cont. Shelf Res. 95, 27–38. https://doi.org/10.1016/j.csr.2015.01.002.

van der Hout, C.M., Witbaard, R., Bergman, M.J.N., Duineveld, G.C.A., Rozemeijer, M.J.C., Gerkema, T., 2017. The dynamics of suspended particulate matter (SPM) and

chlorophyll-a from intratidal to annual time scales in a coastal turbidity maximum. J. Sea Res. https://doi.org/10.1016/j.seares.2017.04.011.

van der Loeff, M.M.R., 1981. Wave effects on sediment water exchange in a submerged sand bed. Netherlands J. Sea Res. 15, 100–112. https://doi.org/10.1016/0077-7579(81)90009-0.

van der Molen, J., Ruardij, P., Greenwood, N., 2017. A 3D SPM model for biogeochemical modelling, with application to the northwest European continental shelf. J. Sea Res. 127, 63–81. https://doi.org/10.1016/j.seares.2016.12.003.

van der Spek, A.J.F., van der Werf, J.J., Grasmeijer, B., Oost, A., Schrijvershof, R., Vermaas, T., 2020. The Kustgenese 2.0 Atlas of the Dutch Lower Shoreface. Delft, the Netherlands.

van der Spek, A., Forzoni, A., Vermaas, T., 2022. Holocene deposits at the lower shoreface and inner shelf of the Dutch coast. Ocean Coast. Manag. 224, 106203 https://doi.org/10.1016/J.OCECOAMAN.2022.106203.

van der Werf, J.J., Schrijvershof, R.A., Brakenhoff, L.B., Grasmeijer, B.T., 2022. Observations of near-bed orbital velocities and small-scale bedforms on the Dutch lower shoreface. Ocean Coast. Manag. 218, 106012 https://doi.org/10.1016/J.OCECOAMAN.2021.106012.

van Duin, E.H.S., Blom, G., Los, F.J., Maffione, R., Zimmerman, R., Cerco, C.F., Dortch, M., Best, E.P.H., 2001. Modeling underwater light climate in relation to sedimentation, resuspension, water quality and autotrophic growth. Hydrobiologia 444, 25–42. https://doi.org/10.1023/A:1017512614680.

van Gerwen, W., Borsje, B.W., Damveld, J.H., Hulscher, S.J.M.H., 2018. Modelling the effect of suspended load transport and tidal asymmetry on the equilibrium tidal sand wave height. Coast. Eng. 136, 56–64. https://doi.org/10.1016/j.coastaleng.2018.01.006.

van Hoey, G., Degraer, S., Vincx, M., 2004. Macrobenthic community structure of soft-bottom sediments at the Belgian Continental Shelf. Estuar. Coast. Shelf Sci. 59, 599–613. https://doi.org/10.1016/J.ECSS.2003.11.005.

van Kessel, T., Winterwerp, H., Van Prooijen, B., Van Ledden, M., Borst, W., 2011. Modelling the seasonal dynamics of SPM with a simple algorithm for the buffering of fines in a sandy seabed. Cont. Shelf Res. 31 https://doi.org/10.1016/j.csr.2010.04.008.

van Maren, D.S., Vroom, J., Fettweis, M., Vanlede, J., 2020. Formation of the Zeebrugge coastal turbidity maximum: the role of uncertainty in near-bed exchange processes. Mar. Geol. 425, 106186 https://doi.org/10.1016/j.margeo.2020.106186.

van Prooijen, B., van Kessel, T., van Ledden, M., 2007. Modelling of fine sediment in a sandy environment-the coastal zone of the Netherlands. In: Proceedings of the Congress: International Association for Hydraulic Research. Venice, Italy, p. 722.

van Rijn, L.C., 1984. Sediment transport, part i: bed load transport. J. Hydraul. Eng. 110, 1431–1456. https://doi.org/10.1061/(ASCE)0733-9429(1984)110:10(1431).

van Rijn, L.C., 2007. Unified view of sediment transport by currents and waves. I: initiation of motion, bed roughness, and bed-load transport. J. Hydraul. Eng. 133, 649–667. https://doi.org/10.1061/(ASCE)0733-9429(2007)133:6(649).

VLIZ, 2022. Sediment profile imaging (SPI). https://www.vliz.be/nl/spi. (Accessed 26 August 2022).

Volkenborn, N., Polerecky, L., Hedtkamp, S.I.C., van Beusekom, J.E.E., De Beer, D., 2007. Bioturbation and bioirrigation extend the open exchange regions in permeable sediments. Limnol. Oceanogr. 52, 1898–1909. https://doi.org/10.4319/LO.2007.52.5.1898.

Walstra, D.J.R., van Rijn, L.C., van Ormondt, M., Brière, C., Talmon, A.M., 2007. The effects of bed slope and wave skewness on sediment transport and morphology. Coast. Sediments '07. https://doi.org/10.1061/40926(239)11. Proceedings.

Webb, J., Theodor, J., 1968. Irrigation of submerged marine sands through wave action. Nature 220, 682–683. https://doi.org/10.1038/220682a0.

Wengrove, M.E., Foster, D.L., de Schipper, M.A., Lippmann, T.C., 2017. Wave and current ripple formation and migration during storms. In: Proceedings of Coastal Dynamics. Helsingør, Denmark, pp. 955–965.

Wengrove, M.E., Foster, D.L., Lippmann, T.C., de Schipper, M.A., Calantoni, J., 2018. Observations of time-dependent bedform transformation in combined wave-current flows. J. Geophys. Res. Ocean. 123, 7581–7598. https://doi.org/10.1029/2018JC014357.

Wengrove, M.E., Foster, D.L., Lippmann, T.C., de Schipper, M.A., Calantoni, J., 2019. Observations of bedform migration and bedload sediment transport in combined wave-current flows. J. Geophys. Res. Ocean. 124, 4572–4590. https://doi.org/10.1029/2018JC014555.

Wiberg, P.L., Harris, C.K., 1994. Ripple geometry in wave-dominated environments. J. Geophys. Res. 99, 775–789. https://doi.org/10.1029/93JC02726.

Widdows, J., Friend, P.L., Bale, A.J., Brinsley, M.D., Pope, N.D., Thompson, C.E.L., 2007. Inter-comparison between five devices for determining erodability of intertidal sediments. Cont. Shelf Res. 27, 1174–1189. https://doi.org/10.1016/j.csr.2005.10.006.

Winterwerp, J.C., 2001. Voorstudie vermindering baggerbezwaar Voorhaven IJmuiden. Delft, the Netherlands.

Winterwerp, J.C., 2007. On the sedimentation rate of cohesive sediment. Proc. Mar. Sci. 8, 209–226. https://doi.org/10.1016/S1568-2692(07)80014-3.

Witbaard, R., Duineveld, G., Bergman, M.J.N., 2013. The final report on the growth and dynamics of *Ensis directus* in the near coastal zone off Egmond, in relation to environmental conditions in 2011–2012. Texel, The Netherlands.

Witbaard, R., Bergman, M.J.N., van Weerlee, E., Duineveld, G.C.A., 2016. An estimation of the effects of *Ensis directus* on the transport and burial of silt in the near-shore Dutch coastal zone of the North Sea. J. Sea Res. 1–10 https://doi.org/10.1016/j.seares.2016.12.001.